(6) STUDIES OF INDIUM-DOPED SILICON.

(9) Semi-Annual Report. 1 Aug 77-31 Jan 78,

by

(10) M.W. Scott, Project Investigator (612) 887-4445
C.E. Jones, Project Scientist (612) 887-4415
R.J. Hager, Research Assistant (612) 887-4505

Honeywell Corporate Material
Sciences Center, Bloomington, MN.

(11) Reporting Period: 1 August 1977 - 31 January 1978 (12) 61 p.

Effective Date: 1 August 1977

Expiration Date: 31 January 1979

Sponsored by

Defense Advanced Research Projects Agency (DoD)
ARPA Order No. 3211
Monitored by NVL Under Contract No. DAAK70-77-C-0194

(14) 47305 (15) ARPA Order-3211

The views and conclusions contained in this document are those of the authors and should not be interpreted as necessarily representing the official policies, either expressed or implied, of the Defense Advanced Research Projects Agency or the U.S. Government.

410 336

UNCLASSIFIED

SECURITY CLASSIFICATION OF THIS PAGE (When Data Entered)

REPORT DOCUMENTATION PAGE		READ INSTRUCTIONS BEFORE COMPLETING FORM
1. REPORT NUMBER DAAK70-77-C-0194	2. GOVT ACCESSION NO.	3. RECIPIENT'S CATALOG NUMBER
4. TITLE (and Subtitle) STUDIES OF INDIUM-DOPED SILICON		5. TYPE OF REPORT & PERIOD COVERED Semi-Annual Report 6. PERFORMING ORG. REPORT NUMBER 47305
7. AUTHOR(s) M. W. Scott C. E. Jones R. J. Hager		8. CONTRACT OR GRANT NUMBER(s) DAAK70-77-C-0194
9. PERFORMING ORGANIZATION NAME AND ADDRESS Honeywell, Inc., Corporate Research Center 10701 Lyndale Ave. So. Bloomington, MN 55420		10. PROGRAM ELEMENT, PROJECT, TASK AREA & WORK UNIT NUMBERS
11. CONTROLLING OFFICE NAME AND ADDRESS MERADCOM Procurement & Production Office Fort Belvoir, VA 22060 Symbol: BYRD/DRDME-PT-3		12. REPORT DATE 1 Aug. 1977 - 31 Jan. 1978 13. NUMBER OF PAGES 59
14. MONITORING AGENCY NAME & ADDRESS (if different from Controlling Office) DCASPRO Honeywell 2701 Fourth Ave. So. Honeywell Plaza Minneapolis, MN 55408		15. SECURITY CLASS. (of this report) Unclassified 15a. DECLASSIFICATION DOWNGRADING SCHEDULE

16. DISTRIBUTION STATEMENT (of this Report)

17. DISTRIBUTION STATEMENT (of the abstract entered in Block 20, if different from Report)

18. SUPPLEMENTARY NOTES

19. KEY WORDS (Continue on reverse side if necessary and identify by block number)

Indium-Doped Silicon; Photoconductive Sensors; X Level; Crystal Growth; Spectroscopy; Hall Measurements

20. ABSTRACT (Continue on reverse side if necessary and identify by block number)

The objectives of this program are to obtain a better understanding of the properties of indium acceptors in silicon, and to develop a new growth procedure which will yield better quality material than is possible by conventional melt-growth techniques.

During this program ~~we have demonstrated~~ was demonstrated the feasibility of growing indium-doped silicon by the gradient-transport solution growth process.

DD FORM 1 JAN 73 1473 EDITION OF 1 NOV 65 IS OBSOLETE

UNCLASSIFIED

SECURITY CLASSIFICATION OF THIS PAGE (When Data Entered)

20. Abstract (Continued)

Eight crystals have been grown over the 1000°C to 1300°C temperature range to determine the Si-In solidus curve. The maximum solubility of indium in silicon was determined to be $1.6 \times 10^{18}/cm^3$ from these measurements.

The peak absorption coefficient due to the indium was found to be 82 cm^{-1} in the crystal grown at 1300°C. Effective-mass-like spectra due to shallower acceptors in both indium and aluminum-doped silicon have been observed for the first time. The spectra corresponds to the indium:X defect at 112.8 meV and to the aluminum:X defect at 56.3 meV. Deep level transient capacitance spectroscopy (DLTS) has been used to measure the trapping parameters of indium acceptors. The capture cross section for holes by the indium centers has been determined to be greater than $10^{-13} cm^2$ at 65K from these measurements.

1/82 cm

1.6 x 10 to the 18 th power/cc

10 to the -13th power sq cm

SUMMARY

The objectives of this program are to obtain a better understanding of the properties of indium acceptors in silicon and to develop a new growth procedure which will yield better quality material than is possible with conventional melt-growth techniques.

During this program we have demonstrated the feasibility of growing indium-doped silicon by the gradient-transport solution growth process. Eight crystals have been grown over the 1000°C to 1300°C temperature range to determine the Si-In solidus curve. The maximum solubility of indium in silicon was determined to be $1.6 \times 10^{18}/cm^3$ from these measurements. Optical absorption measurements have been used as the principal evaluation method to monitor the indium, indium:X, oxygen, carbon, and boron concentrations in the crystals.

The peak absorption coefficient due to the indium was found to be 82 cm^{-1} in the crystal grown at 1300°C. The absorption coefficient is the only unambiguous method for evaluating the crystals, since it is not subject to interpretive models and it provides the information required to determine the quantum efficiency of a photoconductor directly. Effective mass-like spectra due to shallower acceptors in both indium and aluminum-doped silicon have been observed for the first time. The spectra corresponds to the indium:X defect at 112.8 meV and to the aluminum:X defect at 56.3 meV. The aluminum:X defect is being studied in this program since it is believed to have the same origin as the indium:X defect and is experimentally easier to observe and measure. Deep level transient capacitance spectroscopy (DLTS) has been used to measure the trapping parameters of indium acceptors. The capture cross section for holes by the indium centers has been determined to be greater than $10^{-15}cm^2$ at 65K from these measurements.

A paper entitled "Infrared Spectra of New Acceptor Levels in Indium- or Aluminum-Doped Silicon" has been submitted for publication.

TABLE OF CONTENTS

LIST OF ILLUSTRATIONS

LIST OF ILLUSTRATIONS (Concluded)

LIST OF TABLES

SECTION 1
INTRODUCTION

There is need for improvement in the performance/cost ratio capabilities of infrared detection systems. The need is especially great for Army applications. A promising approach toward satisfying this requirement is the development of high-performance infrared focal planes, consisting of integrated sensors combining detector arrays and signal-processing electronics. The most desirable focal plane would consist of a detector array and electronics fully integrated as a monolithic sensor.

Recently, indium-doped silicon has been investigated as an extrinsic detector material for use in advanced infrared imaging systems. A number of problems have arisen with this material, notably with the uniformity of the crystals and the temperature of operation of the device.

Present growth techniques are not adequate to produce the high quality material necessary for extrinsic detectors. Czochralski-grown material suffers from resistivity striations, swirl defects, and excessive amounts of unwanted impurities such as B and C. Float-zoned crystals can be made more uniform and with lower concentrations of residual impurities; however, the indium-doping level is inadequate for high quantum efficiency photoconductors because of the low segregation coefficient of indium.

Problems with the low operating temperature of indium-doped silicon detectors have been attributed to a shallow X defect level associated, in some way, with indium. Observation of this X defect level has relied on complex computer fitting of Hall measurements, but has eluded other types of measurements. We have now been able to directly observe this defect with infrared absorbance measurements. An anomalous shallower defect has also been observed in aluminum-doped silicon, indicating that this may be a problem characteristic of all the Group IIIA acceptors in silicon.

The purpose of this program is to determine the origin and limitations of the shallow acceptor levels associated with indium and other Group IIIA acceptors in silicon. The specific objectives are two-fold:

(a) to develop a better understanding of indium acceptors in silicon, and
(b) to develop a new growth process which can produce better quality indium-doped silicon for photoconductors than is achievable by Czochralski growth.

The major milestones which we have been working toward during this portion of the contract have been to:

(a) determine the maximum solubility of indium in silicon
(b) determine the recombination coefficient for indium acceptors, and
(c) determine the origin of the X defect in indium-doped silicon.

SECTION 2
EXPERIMENTAL PROCEDURES

2.1 SOLUTION GROWTH

A schematic illustration of the growth apparatus which was originally used is shown in Figure 1. It consists of a flat-bottomed quartz tube in which was placed a single crystal silicon seed, high purity (6N) indium, and a high purity silicon source in the relative positions shown in Figure 1. A tubular quartz spacesd to hold the silicon seed in place during the growth and prevent it from buoying to the surface of the liquid indium. The apparatus is placed in a furnace with a uniform temperature profile and a temperature difference is established between the silicon source, at temperature T_H, and the substrate, at temperature T_L, by a flow of air directed at the flat bottom of the ampul. The temperature of the silicon seed is maintained approximately 50°C colder than the source temperature throughout the growth process.

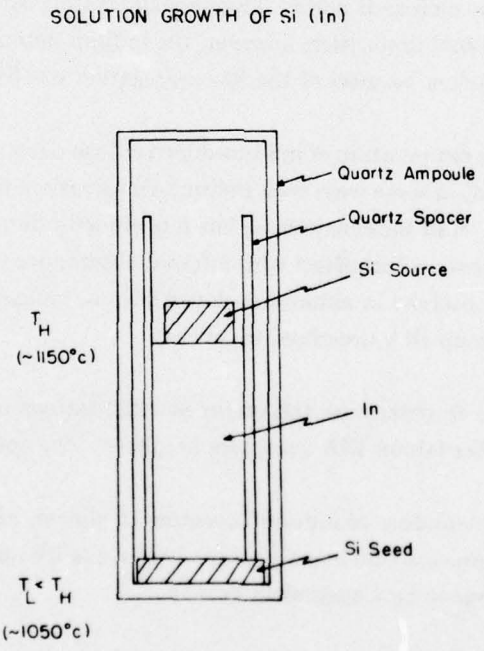

Figure 1. Schematic of Solution Growth Apparatus

The temperature difference between source and substrate was determined by calibrating the system using a Pt-Pt (3h) thermocouple. The capsule was loaded with the usual amount of indium and a standard substrate. A quartz tube containing the thermocouple was inserted into the indium to be in contact with the substrate. The apparatus was brought up to temperature, and the temperature profile in the indium measured. The profile was measured with the gas flow rate a parameter in order to obtain any desired temperature difference across the indium column. The flow required to maintain a 50°C temperature difference was determined in this way. The repeatability of the temperature setting was estimated at about ±5°C from these measurements.

Modifications and variations in the basic growth apparatus occurred during the course of the contract. Most importantly, we have eliminated the quartz spacer from the ampul. It was determined that the major source of boron contamination in the solution-grown crystals came from the ends of the spacer. The seed could be held in place by putting dents in the ampul wall. Also, an open tube system with an argon atmosphere was used at the higher temperatures to prevent collapsing of the ampul.

2.2 HALL MEASUREMENTS

Hall measurements were made in a dc mode at a field of 8KG. The system uses a Janis Model 8DT research dewar which can be cooled to liquid He temperatures. The sample temperature can be controlled to 0.1°K with a Lakeshore Cryotronics DT-500 temperature controller. The system can measure either bridge-type or van der Pauw configuration samples up to a resistance of 10^9 ohms, but only bridge-type configurations up to 10^{13} ohms.

The samples were all made in a bridge configuration using evaporated aluminum as the contact. The contact was annealed at 750°C for 45 min in hydrogen to alloy the aluminum. Contact to the aluminum was made with ultra-sonically soldered indium.

2.3 OPTICAL MEASUREMENTS

The procedures used are explained in the publication presented in Appendix B.

2.4 DLTS SYSTEM

The DLTS technique measures the effect traps have on the transient capacitance of a sample diode after a voltage pulse. A block diagram of the apparatus is shown in Figure 2. The major parts of the apparatus include a dewar capable of varying the temperature from 4 to 400K, electronics for applying a bias and sharp voltage pulses to the sample, a fast capacitance bridge for measuring the transient effects, and a double box-car which measures the amplitude and time constant for each transient component.

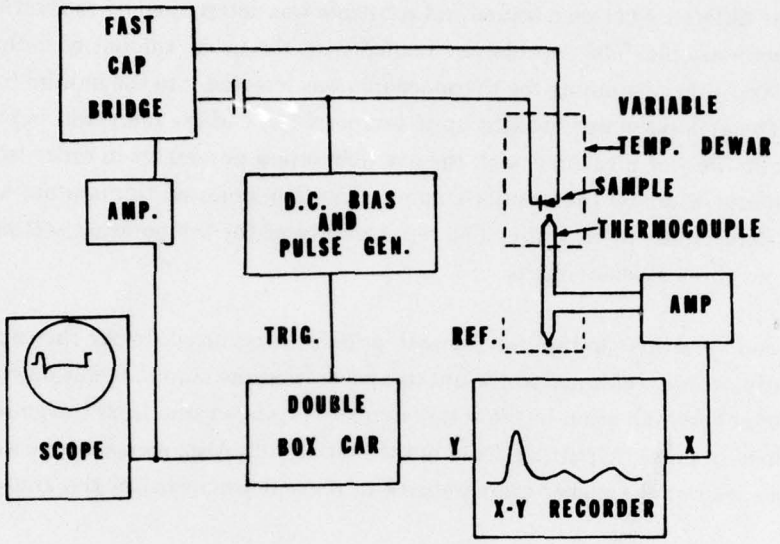

Figure 2. Block Diagram of the DLTS Apparatus

2.5 JUNCTION FABRICATION

The sample is a diode made by diffusing boron and phosphorous into an indium-doped crystal. The structure is shown in Figure 3. The boron and phosphorous provide free carriers which can be trapped on the indium centers. The capacitance of the reverse biased diode provides the effect which is used to study this trapping.

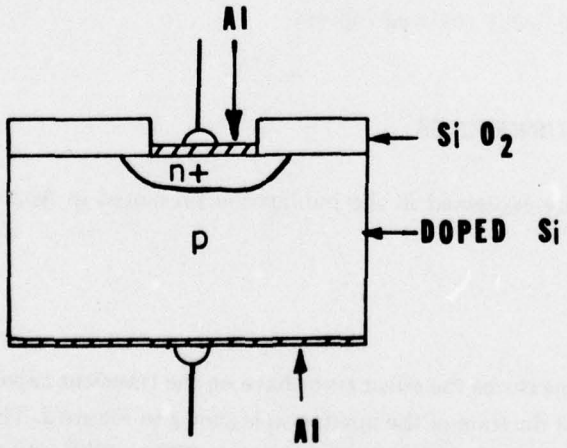

Figure 3. The structure of test diodes used to study indium trapping by the DLTS technique. The concentrationsa are $N_p >> N_B > N_{In}$.

SECTION 3
RESULTS AND DISCUSSION

3.1 GRADIENT TRANSPORT SOLUTION GROWTH

3.1.1 Description of Process

The sequence of events leading to the growth of indium-doped silicon is basically the following. When the ampule shown in Figure 1 is brought up to temperature, silicon is dissolved into the indium at both the top (source) and bottom (substrate). The solubility limit of silicon at the top is C_H (expressed in appropriate units) and at the bottom is C_L, with $C_H > C_L$ because of the higher temperature at the top. As a result, the indium in contact with the silicon at the top will be doped to a concentration of C_H with silicon, and the bottom layer will be doped to a concentration of C_L with silicon. Because of the concentration gradients of silicon in the indium, silicon will diffuse away from both the source and substrate, dissolving these two crystals. At some time after the start of this process, the concentration gradient will drive the silicon in the direction of the substrate everywhere in the melt, and the substrate will cease dissolving in the indium. Since the silicon concentration at the liquid-solid interface is at the solubility limit, any silicon transporting to the substrate will precipitate on the substrate. The material grown in this way will contain the maximum amount of indium possible (i.e., the solubility limit of indium) at the temperature T_L.

3.1.2 Theory

This section presents a more precise treatment of the growth process, including the relevant parameters and a mathematical model of the diffusion process. Exact solution of the diffusion equation is possible, from which various parameters (such as the average growth rate) can be computed.

The transport of silicon to the substrate is governed by the usual diffusion equation

$$\frac{\partial C_{Si}}{\partial t} = D\nabla^2 C_{Si} \tag{1}$$

where C_{Si} is the concentration of silicon in the melt and D is the diffusion coefficient in the melt.

The boundary conditions we have to solve equation (1) are:

$C_{Si}(x,t) = C_o$ at $x = 0$ (source)

$C_{Si}(x,t) = C_\ell$ at $x = \ell$ (substrate)

$C_{Si}(x,o) = 0$ initially.

In this form we have assumed the origin to be at the source, a column of length l, and no silicon in the melt to begin with. In addition we have assumed the problem to be one dimensional and that the finite size of the source, substrate, and quartz apparatus has no effect. We also assume that the source and substrate surfaces remain fixed relative to each other during the growth, which is not strictly true in the procedure we use.

The diffusion equation with the above boundary conditions has the solution:

$$C_{Si}(x,t) = C_o - (C_o - C_\ell)\frac{x}{\ell} + \frac{2}{\pi}\sum_{1}^{\infty}\frac{C_\ell \cos m\pi - C_o}{m}\sin\frac{m\pi x}{\ell}\, e^{-m^2\pi^2 Dt/\ell^2} \tag{2}$$

Examining equation (2) it is clear that as $t \to \infty$, the concentration approaches a linear variation with x, i.e.,

$$C(x, t \to \infty) = C_o - (C_o - C_\ell)\frac{x}{\ell} \tag{3}$$

which is expected in the steady state. Except for small times, only the first term in the sum is important. Therefore, the equation can be approximated by:

$$C_{Si}(x,t) = C_o - (C_o - C_\ell)\frac{x}{\ell} - \frac{2}{\pi}(C_o + C_\ell)\sin\frac{\pi x}{\ell}\, e^{-y} \tag{4}$$

where $y = \dfrac{\pi^2 Dt}{\ell^2}$

The concentration profiles of silicon in the indium are shown in Figure 4 for times of 1, 3, and 6 hours after the start of growth. The conditions used in the figure were $T_H = 1050°C$, $T_L = 1000°C$, and a length l = 3 cm. After 6 hours the concentration gradient drives the material toward the substrate, and growth begins.

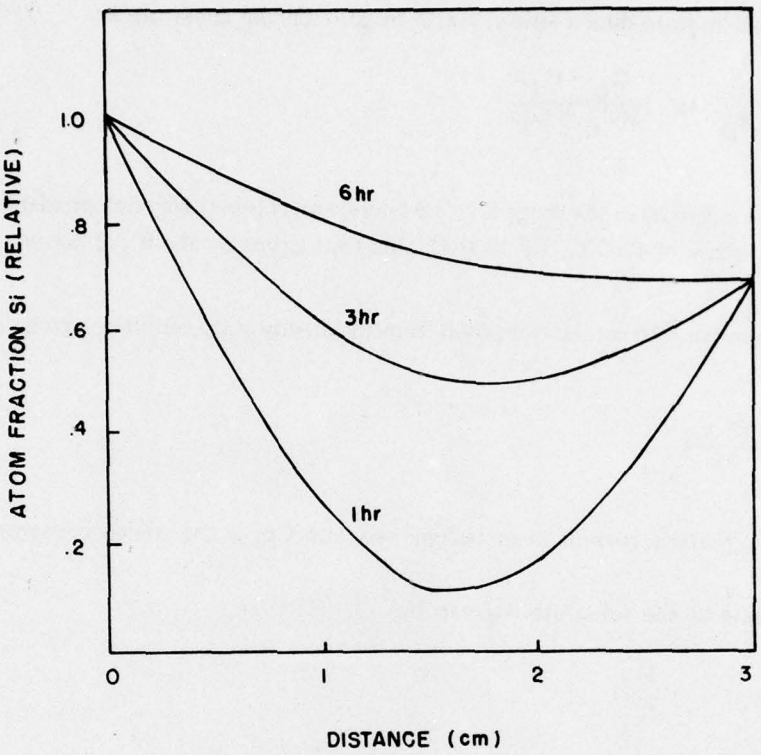

Figure 4. Concentration Profile of Silicon in the Indium Solution at Various Times for a Capsule at 1050°C Source Temperature

The solubility of silicon in indium (i.e., the Si-In liquidus curve) has to be known in order to calculate these profiles. This information was obtained from the literature and is presented in Appendix A of this report.

The following sections present some of the relevant parameters, such as time to start growth and the average growth rate, in analytic form.

The crystal begins growing on the substrate when the mass transport is in the direction of the substrate everywhere in the ampul; i.e., when

$$\frac{dC_{Si}}{dx} < 0 \text{ at } x = \ell$$

This condition is satisfied when

$$e^{-y} = \frac{C_o - C_\ell}{2(C_o + C_\ell)}$$

The time before indium-doped silicon starts to grow on the substrate is:

$$t_G = -\frac{\ell^2}{\pi^2 D} \ln \frac{C_o - C_\ell)}{2(C_o + C_\ell)} \tag{5}$$

The time turns out to be in the range 5.7 - 5.9 hours, and is practically independent of temperature up to a growth temperature of 1200°C. By 1300°C, this time drops to about 3.2 hours.

The average growth rate can be computed from the steady state conditions given in equation (3) and the condition

$$J = - D \frac{\partial C_{Si}}{\partial x}_{x=\ell}$$

where J is the particle current in moles/cm^2 sec, and C_{Si} is the silicon concentration in moles/cm^3.

The growth rate at the substrate is given by

$$\overline{V}(cm/sec) = J \frac{M_{Si}}{\rho_{Si}}$$

where M_{Si} is the molar weight of silicon,
ρ_{Si} is the density of the silicon crystal.

Using equation (3), the average (or steady state) growth rate, this can be written:

$$\overline{V}(cm/sec) = + D \frac{M_{Si}}{\rho_{Si}} \frac{(C_o - C_\ell)}{\ell} \tag{6}$$

The average growth rate depends on the concentration gradient in the indium and the diffusion rate of silicon through the indium. In order to characterize the growth process completely, we need to know only two parameters:

(a) the diffusion coefficient, D, and
(b) the Si-In liquidus.

As mentioned previously, the Si-In liquidus curve used in the calculations is included in Appendix B.

The diffusion coefficient in liquid indium has been measured up to 1000°C.[1] The diffusion coefficient is given by the expression

$$D = 3 \times 10^{-4} \exp -\left(\frac{2.5 \text{ kcal/mole}}{RT}\right) \text{cm}^2/\text{sec}$$

Over the temperature range of interest in our growth experiments (1000°C to 1350°C) this variation is relatively small. For convenience we use the value 1×10^{-4} cm²/sec, which is approximately the upper limit for D in this temperature range.

3.1.3 Comparison with Experiment

The predicted growth rates are shown in Figure 5 as a function of the growth temperature. The temperature difference between source and substrate was assumed to be 50°C at all growth temperatures, and the spacing was 3 cm. The growth rate increases dramatically with increasing growth temperature up to about 1300°C. Referring to the liquidus curve in Appendix A, one can see that dC/dT is a maximum near 1300°C, accounting for the maximum in growth rate. The maximum expected rate is in the 10-20 mm/day range, which is more than adequate to produce the material needed for infrared focal planes.

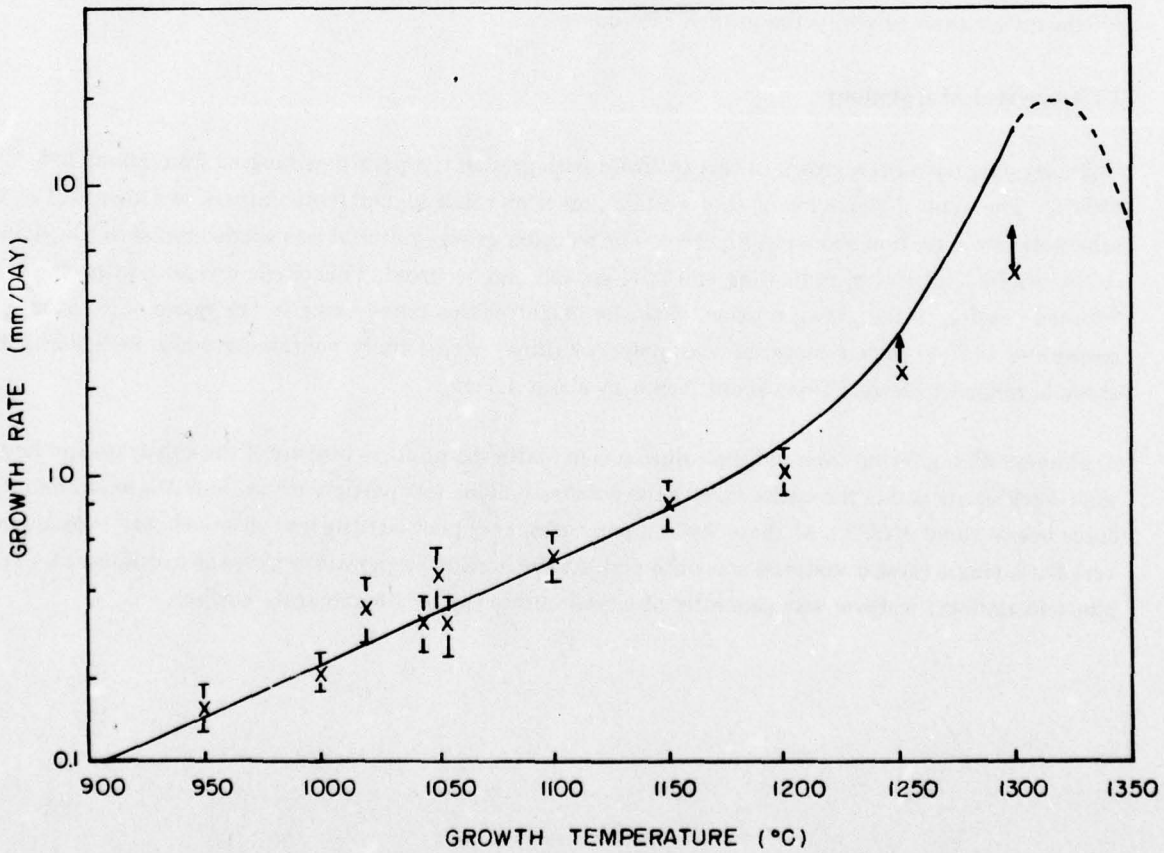

Figure 5. Growth Rate as a Function of the Substrate Temperature and a 50°C Temperature Difference

The experimentally determined growth rates are also shown in Figure 5. Some of the lower temperature growths were done on Honeywell funding, but are shown here for completeness. In general the measured values agree very well with theoretical values, indicating that reasonable values of the parameters were used in the calculation. The errors assigned to the growth rates result from partial melt-back of the substrate. Usually it was difficult to determine precisely how much melt-back occurred before the growth started. As a result, we determined both the maximum and minimum rates, corresponding to either complete melt-back or no melt-back of the substrate. The value shown in Figure 5 is then the average. Some error also occurs in determining the length of time of the growth, since it requires some time for steady state to be reached. The growths were typically about 10 days, so this is judged to be only a small error.

The growth runs at 1250°C and 1300°C are believed to be only lower limits to the actual growth rates. In both cases the source material did not feed into the solution properly during growth. There is a tendency for the quartz ampul to collapse at these higher temperatures, trapping the source out of the indium. We did not repeat these growth runs since the primary objective was to determine the solubility of indium in silicon rather than to verify the growth rate curve.

3.1.4 Crystal Morphology

Eight crystals have been grown in this program with growth temperatures ranging from about 1000°C to 1300°C. The typical behavior of the crystals grown at these higher temperatures is illustrated in the schematic cross section shown in Figure 6. The solution-grown material was single crystal in the vicinity of the original substrate, indicating epitaxial growth had occurred. This single crystal portion formed a "domed" region in the grown portion, with the height of this dome being in the range of 2-7 mm. The remaining indium-doped material was polycrystalline, occasionally containing some inclusions. The crystals ranged in length from about 5 mm to about 1.7 cm.

A problem with growing from indium solution is in obtaining uniform wetting of the substrate and having melt-back occur across the entire face of the substrate. This was particularly serious at growth temperatures below about 1050°C. At these low temperatures, very poor wetting was observed, and consequently very little single crystal material was obtained. At the higher temperatures this was much less of a problem and uniform wetting was generally observed across the entire substrate surface.

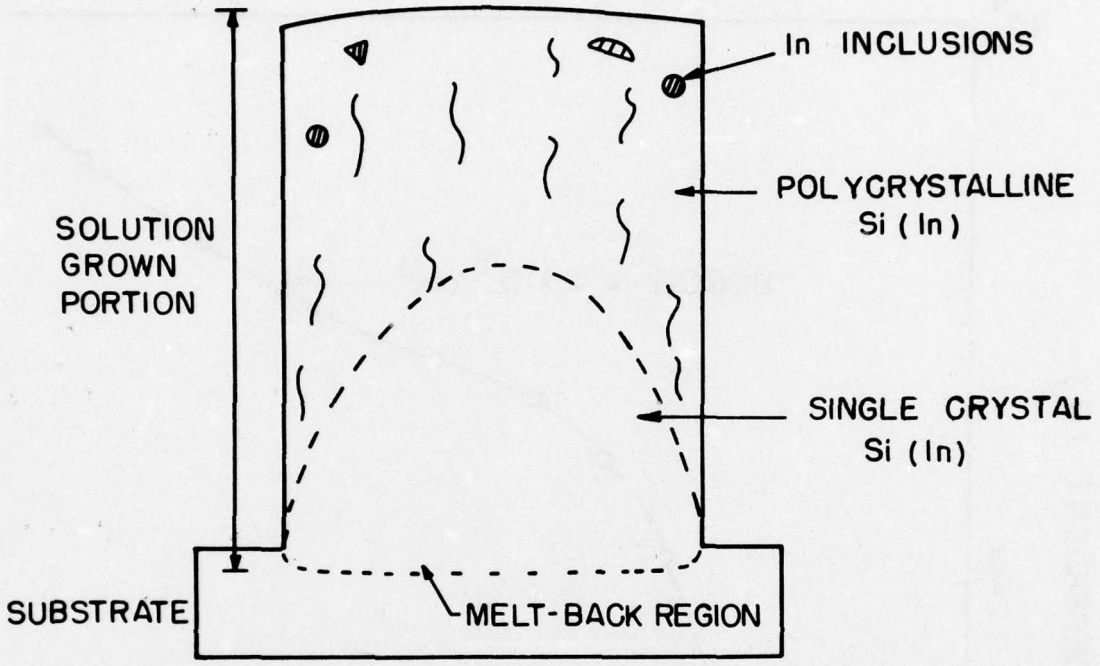

Figure 6. Schematic Cross Section of the Solution-Grown Crystals

3.2 CRYSTAL EVALUATION

3.2.1 Hall Measurements

All the crystals grown under this program have been characterized by Hall effect measurements versus temperature on at least one sample from each growth. An example of the types of curves obtained are shown in Figures 7 and 8. The Hall curves have a slope of $E_{IN/2}$ at the higher temperatures and slopes of E_B or E_x at the lower temperatures. The boron concentration was estimated from the knee in the Hall curve, as illustrated in Figure 7.

The Hall curve shown in Figure 8 was measured on the crystal grown at 1300°C and corresponds to the most heavily doped crystal grown in this program. The high temperature portion also shows an $E_{In/2}$ slope, but the low temperature portion is characteristic of the indium:X defect at an activation energy of 0.1 eV. A detailed fit of the Hall coefficient versus temperature was not attempted during this phase of the program.

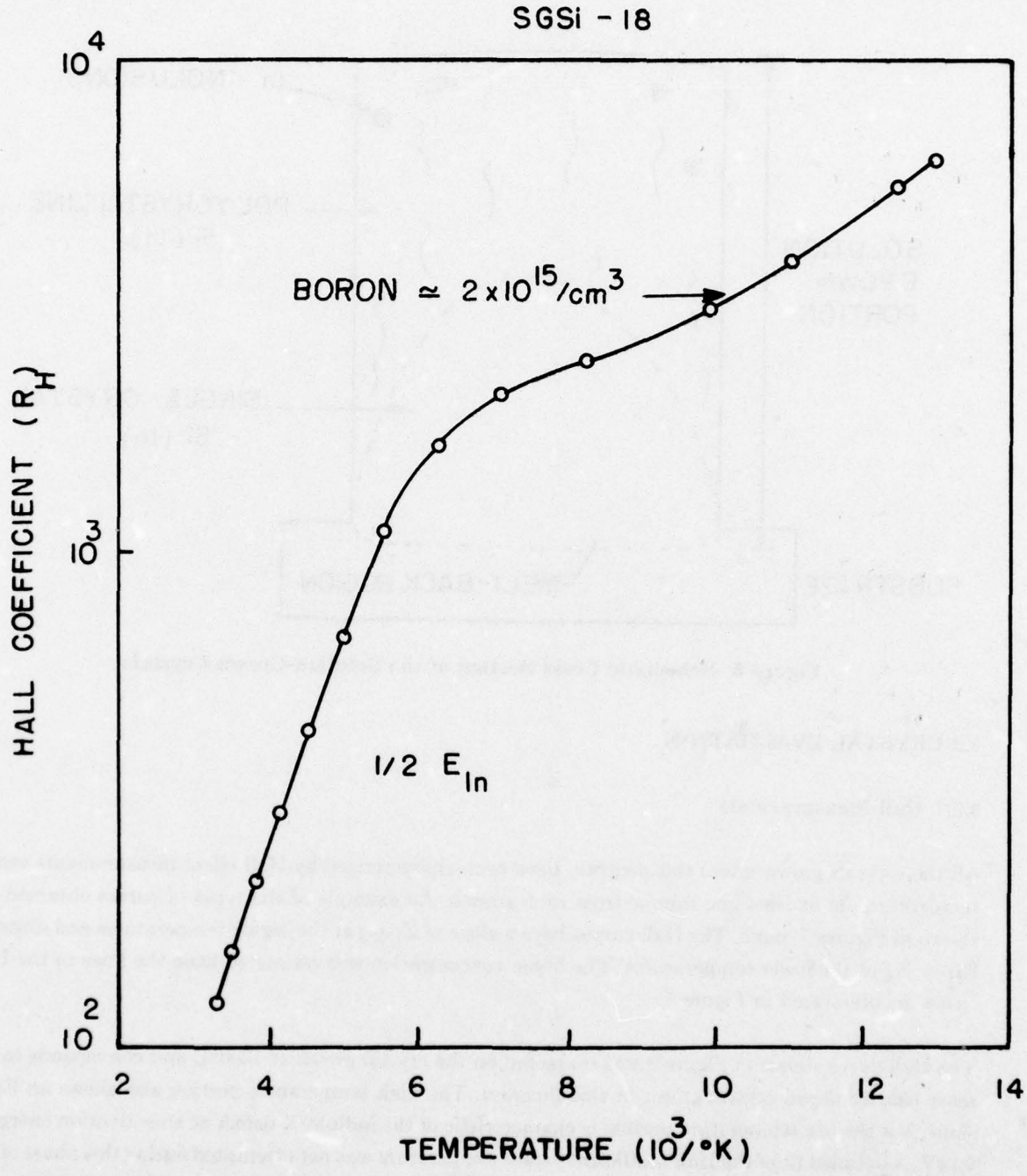

Figure 7. Hall Coefficient versus Reciprocal Temperature for Crystal SGSi-18

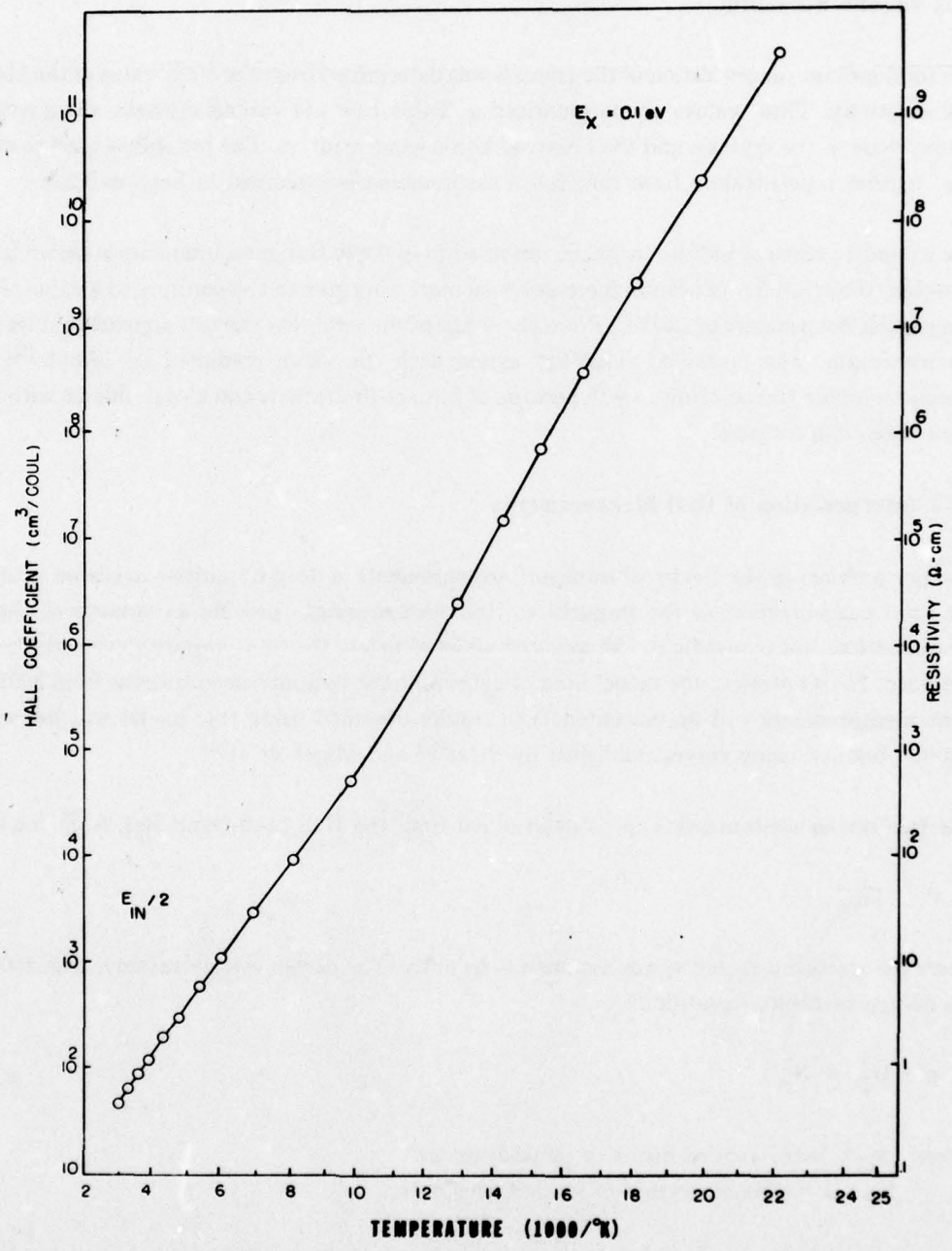

Figure 8. Hall Coefficient versus Reciprocal Temperature for Crystal SGSi-22

3.2.2 Indium Solubility

The total indium concentration of the crystals was determined from the 300K value of the Hall coefficient and resistivity. These values are summarized in Table I for the various crystals, along with the growth temperature of the crystals and the observed boron concentration. The procedure used to determine the total indium concentration from the Hall measurements is explained in Section 3.2.3.

The solubility curve of indium in silicon obtained from 300K Hall measurements is shown in Figure 9. As expected, the solubility of indium increases with increasing growth temperature to a value of $1.6 \times 10^{18}/cm^3$ at a growth temperature of 1300°C. From the shape of the solubility curve it appears that we are very near the maximum. The measured solubility agrees with the value predicted by Marsh.[3] We did not attempt a higher temperature growth because of furnace limitations and also problems with the quartz at these high temperatures.

3.2.3 Interpretation of Hall Measurements

A major problem in the electrical transport measurements of deep impurities in silicon is in determining the total concentration of the impurities. Hall measurements provide a measure of the free carrier concentration, but a specific model must be adopted before the total impurity concentration can be determined. In this section, the model used to determine the indium concentrations from 300K Hall coefficient measurements will be presented. The results obtained using this model will be compared with results obtained using curves published by Sclar[2] and Marsh et al[3].

The free carrier concentration, p, is determined from the Hall coefficient, R_H, from the expression

$$p = \frac{r}{eR_H}$$

where the scattering factor, r, was assumed to be unity. The carrier concentration is also determined from the charge neutrality condition.

$$p + N_D^+ = N_A^- \tag{7}$$

where: N_D^+ is the concentration of ionized donors
N_A^- is the concentration of ionized acceptors.

By assuming a low donor concentration and a high concentration of indium relative to any other acceptor, this can be rewritten as

Table I. Summary of Electrical Evaluations

Crystal	Growth T(°C)	R_H(300) cm^3/C	R(300) Ω-cm	μ(300) cm^2V-s	[In] cm^{-3}	[B](Hall) cm^{-3}
9	1005	281	1.28	220	$6x10^{16}$	
11	946	620	2.17	285	$1.8x10^{16}$	
12	1056	169	0.597	284	$1.5x10^{17}$	$2x10^{15}$
14	1056	198	0.74	275	$1.14x10^{17}$	
15	1008	317	1.03	302	$5.2x10^{16}$	$1x10^{14}$
17	1056	213	0.745	286	$1x10^{17}$	$5x10^{14}$
18	1100	122	0.435	257	$2.8x10^{17}$	$1.5x10^{15}$
19	1150	87.5	0.36	243	$5.1x10^{17}$	$1.0x10^{15}$
20	1200	62.4	0.244	223	$1.0x10^{18}$	$6.3x10^{15}$
21	1250	35.3	0.179	198	—	$6.3x10^{16}$
22	1300	45.5	0.238	191	$1.6x10^{18}$	—
23	1250	52.5	0.255	206	$1.4x10^{18}$	—

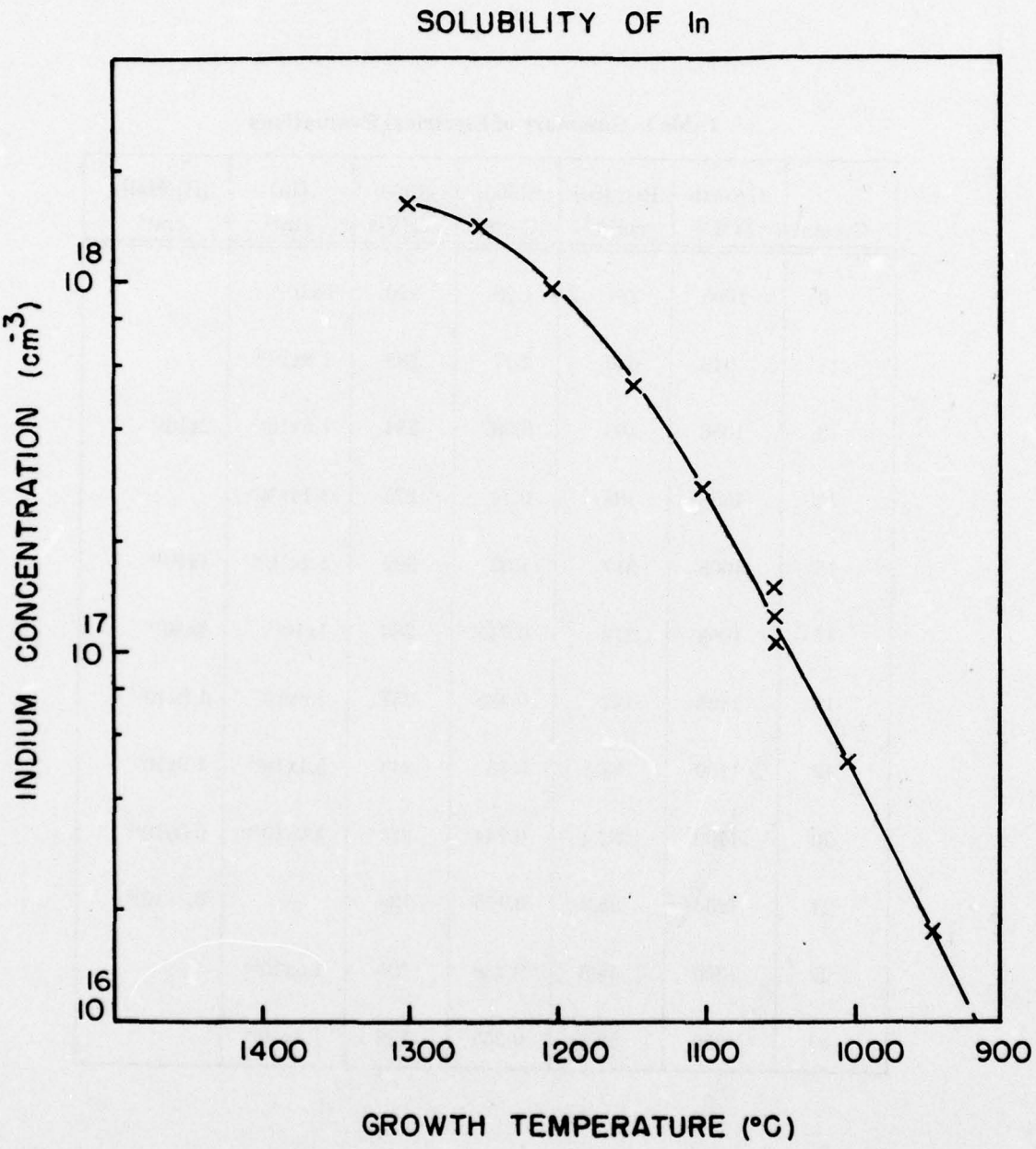

Figure 9. Indium Concentration as a Function of Growth Temperature

$$p = \frac{N_{In}}{1+g \exp \frac{E_i - E_F}{KT}} \tag{8}$$

where: N_{In} is the total In concentration
g is the ground state degeneracy
E_i is the In ionization energy
E_F is the Fermi energy.

In this expression the effects of the indium-excited states have been ignored, and only the ground state is considered.

The hole concentration can also be determined from the usual expression for non-degenerate bands,

$$p = \frac{N_v}{1+ \exp \frac{E_F}{KT}} \tag{9}$$

where N_v is the effective density of states in the valence band.

Equations (8) and (9) can be used to determine the Fermi energy and subsequently the hole concentration as a function of the total indium concentration.

The values of the various parameters used are the following:

$N_v = 4.8296 \times 10^{15} (m_h^*/m_o\ T)^{3/2}$

$m_h^* = 0.81$ at 300K [4]

$E_i = 0.155$ eV

$g = 4$

The curve of 300K hole concentration as a function of the indium concentration is shown in Figure 10. At the low concentrations of indium the impurities are nearly totally ionized, but at high concentrations the degree of ionization drops dramatically. At 10^{18} In/cm^3, for example, only 10 percent of the centers will be ionized at 300K.

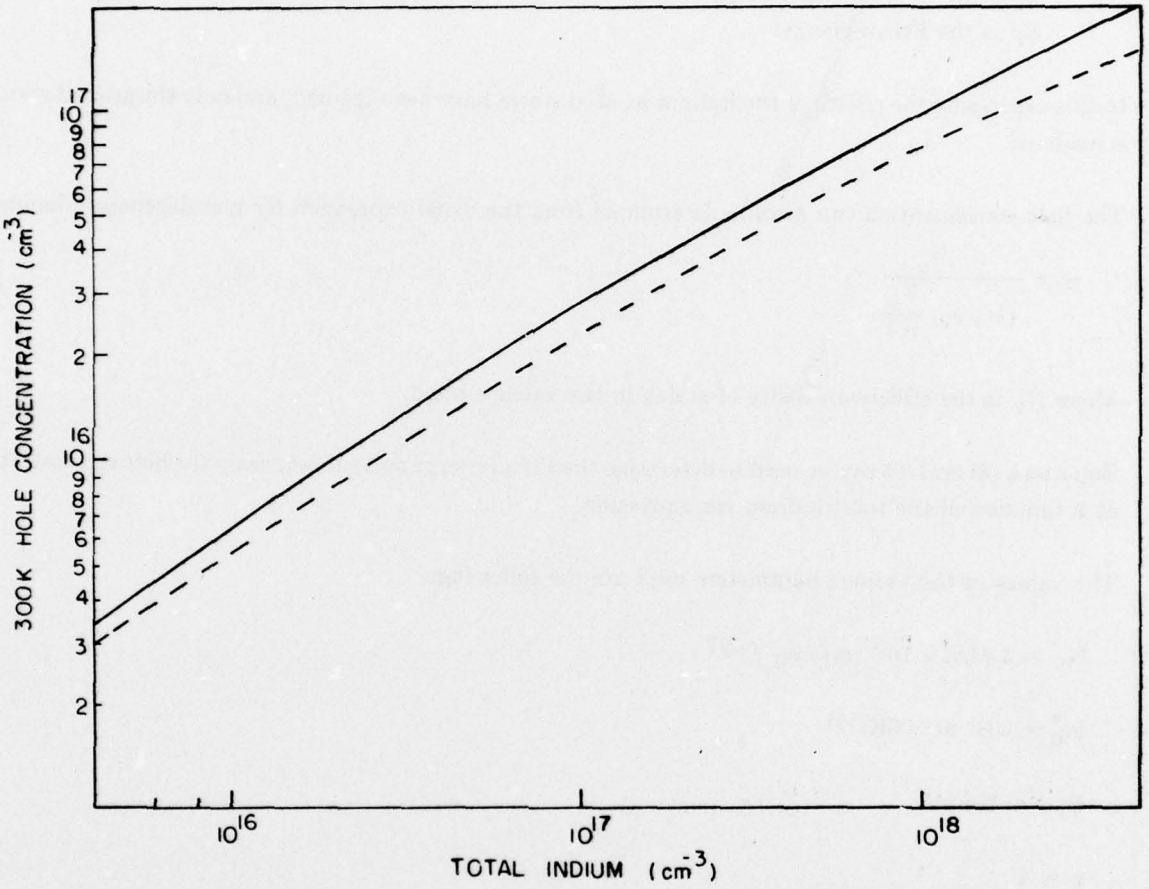

Figure 10. Hole concentration at 300K as a function of the total indium concentration. The dashed curve is from Sclar; the solid curve is used in this report.

Recently, Sclar[2] published calculations of the expected degree of ionization of deep impurities in silicon at 300K. The curve obtained from his work is also shown in Figure 10 as the dashed curve. The main feature to note is that his curve predicts a greater indium concentration in a crystal for any measured 300K hole concentration. In other words, the curve published by Sclar overestimates the amount of indium in a crystal. It appears that this discrepancy arises from the effective mass values he used. We have used the more recent value of $0.81m_o$ for the 300K density of states effective mass.

Marsh et al[3] have also arrived at a means of determining the total indium concentration based on a computer fit to Hall coefficient measurements. Their data appear to agree with the published curve of Sclar over most of the range of indium concentrations. Their data agree with Sclar's curve to within ± 10 percent at the high doping levels, so we see no basic difference in those two determinations.

In his paper, Sclar also computed the variation in 300K resistivity with total indium concentration. This curve is reproduced in Figure 11, along with a similar curve proposed by Marsh et al.[3] Both curves predict a different variation of resistivity with doping level, particularly at concentrations in the $1\text{-}2\times10^{17}/cm^3$ range, with the two curves crossing at indium concentrations of about $1.5\times10^{18}/cm^3$ and $2\times10^{16}/cm^3$. The circles shown in the figure are the values of resistivity and indium concentration obtained from our measurements and listed in Table I. It is obvious that our values agree with Sclar's curve better than with Marsh's.

There is a discrepancy in our calculations compared with Sclar's which has not been resolved yet. The degree of ionization which Sclar computes does not agree with our calculation, but yet the total indium concentration obtained from the resistivity data does agree with our calculations. Clearly, the interpretation of indium concentration from electrical measurements is subject to the particular model invoked. In determining the total indium concentration, we will use the curve shown in Figure 10. In order to remove the discrepancy which exists in evaluating Si(In) crystals, a different method should be used. Since optical absorption is the final desired result in these crystals, the peak absorption coefficient due to the indium would be a useful criterion. This point is discussed in Section 3.3.1.

3.3 OPTICAL EVALUATION

One of the primary means of evaluating the solution-grown material and characterizing the shallower X defects in aluminum and indium crystals has been by optical absorbance measurements. Optical absorption has been measured on all of the crystals grown in this program, with the exception of crystal SGSi21. The boron concentration in this crystal was too high to make the optical measurements worthwhile.

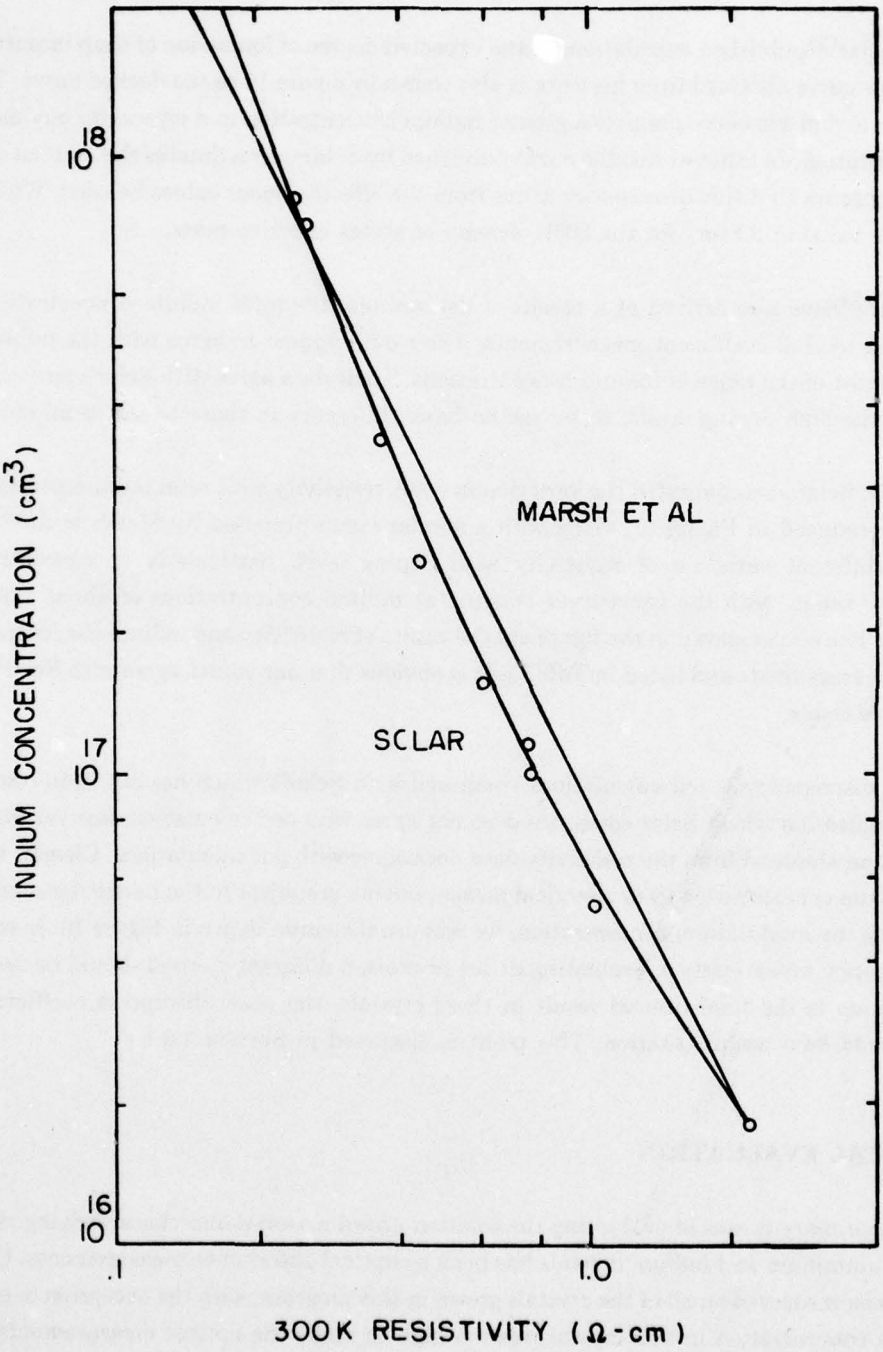

Figure 11. Total Indium Concentration as a Function of 300K Resistivity

3.3.1 Absorption in Indium-Doped Silicon

The absorption spectrum of indium-doped silicon in the 400 cm^{-1} to 2000 cm^{-1} (25 μm to 5 μm) region is shown in Figure 12, as an illustration of the optical measurements. The principal indium lines are marked as lines 1, 2 and 4, to be consistent with the numbering system used by Onton et al[5] for acceptors in silicon. The other sharp absorption line identified is due to oxygen. The broad absorption bands in the 400 to 1000^{-1} region are lattice absorptions, and the broad absorption starting at 1200 cm^{-1} is due to ionization of the indium centers.

The region of interest for monitoring the indium:X defect is between 700 and 1000 cm^{-1}, right where there is appreciable lattice absorption. The spectrum with the lattice absorption bands subtracted away is shown in Figure 13. Again, the principal absorption lines have been identified as in the previous figure. In this case additional lines due to oxygen at 516 cm^{-1} and carbon at 606 cm^{-1} are clearly seen. The peak absorption coefficient of about 5 cm^{-1} for this crystal is also indicated in Figure 13. The peak absorption due to the indium occurs at an energy of about 2400 cm^{-1} and is used as a measure of the total indium concentration in the crystal.

The absorption spectra of three crystals measured in this program in the 400 to 1300 cm^{-1} region are shown in Figures 14, 15 and 16. The spectrum in Figure 14 is from a Czochralski crystal with 2.8×10^{17} In/cm^3 and the spectrum in Figure 15 is a solution-grown crystal with the same indium concentration (crystal SGSi-18). The various lines are labelled in each case: oxygen, carbon, boron and the indium:X defect. The major point to note is the much stronger absorption due to the indium:X defects in the Czochralski crystal as compared with the solution-grown crystal, indicating a much higher concentration.

A number of other features should be pointed out before further discussion of the indium:X defect. In particular, note that the boron concentration can be monitored in the crystals. From the relative magnitudes of the 670 cm^{-1} boron line, the relative concentrations can be determined in the various crystals. Absolute concentrations are estimated based on a previously measured integrated cross section of 4×10^{-15} cm for this line. Boron also introduces additional structure in the spectrum in the 700 to 900 cm^{-1} region which interferes with the indium:X lines, as seen in Figure 16.

The absorption spectrum of crystal SGSi-22, doped with 1.6×10^{18} In/cm^3, is shown in Figure 16. The background absorbance is much higher in this crystal compared with that of more lightly doped crystals, indicating that excited state banding is starting to occur. Note that we are using a sensitive scale on the ordinate in Figure 16, so that this "smearing-out" of the excited state absorption lines is still relatively insignificant. The indium:X absorption lines are clearly seen in this crystal, along with the usual oxygen and carbon lines. The exception is that no boron absorption was observed in this crystal, making the concentration less than 5×10^{13}/cm^3.

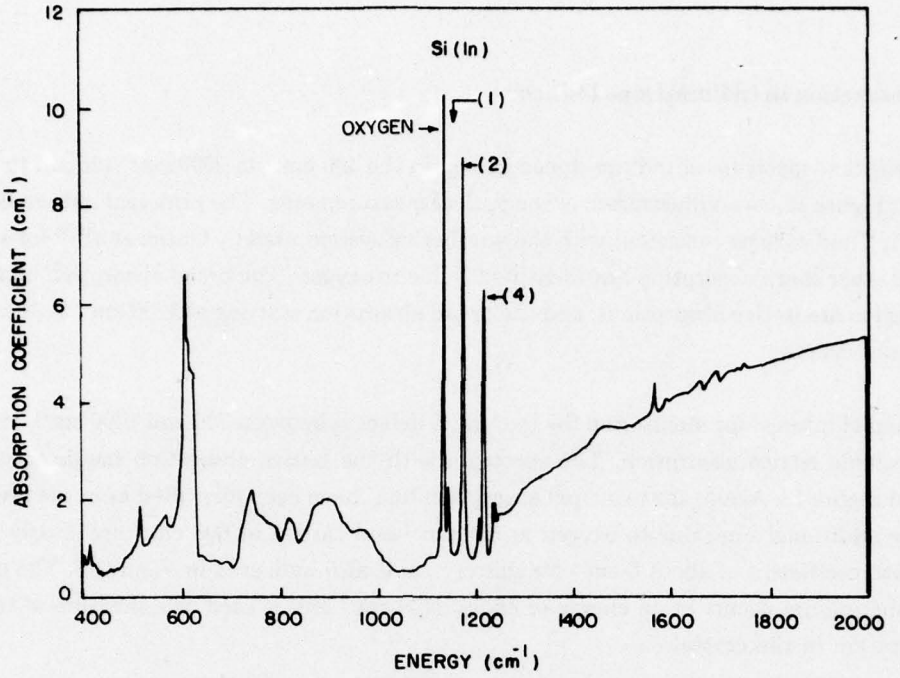

Figure 12. Absorption Spectrum in Indium-doped Silicon at 8K

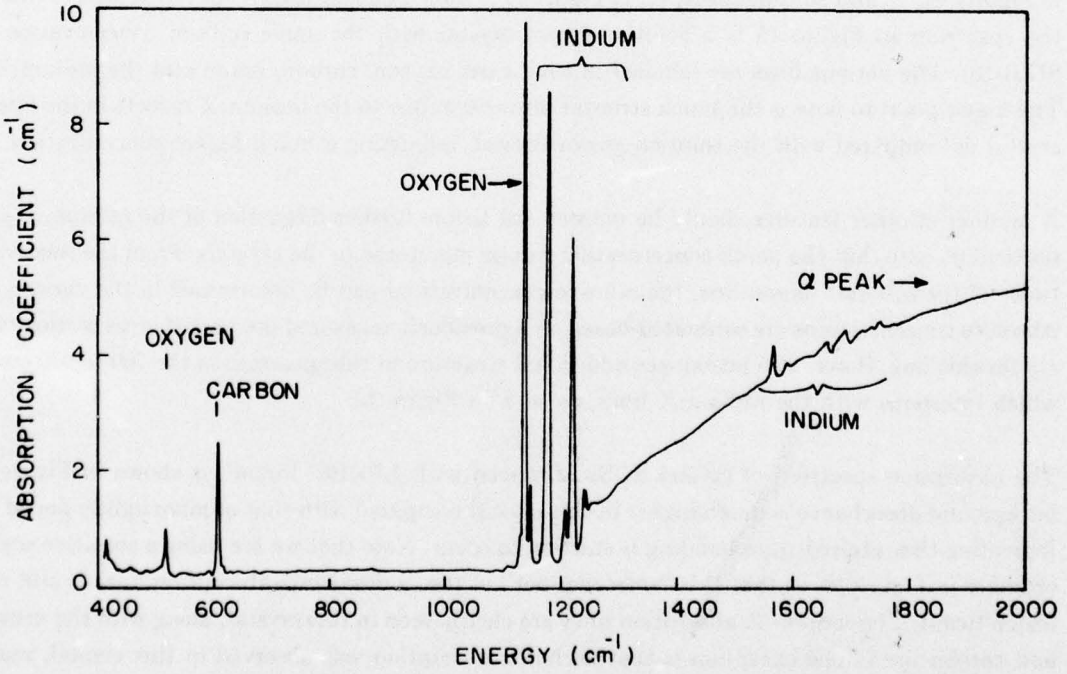

Figure 13. Absorption Spectrum in Indium-doped Silicon with the Lattice Absorption Bands Subtracted

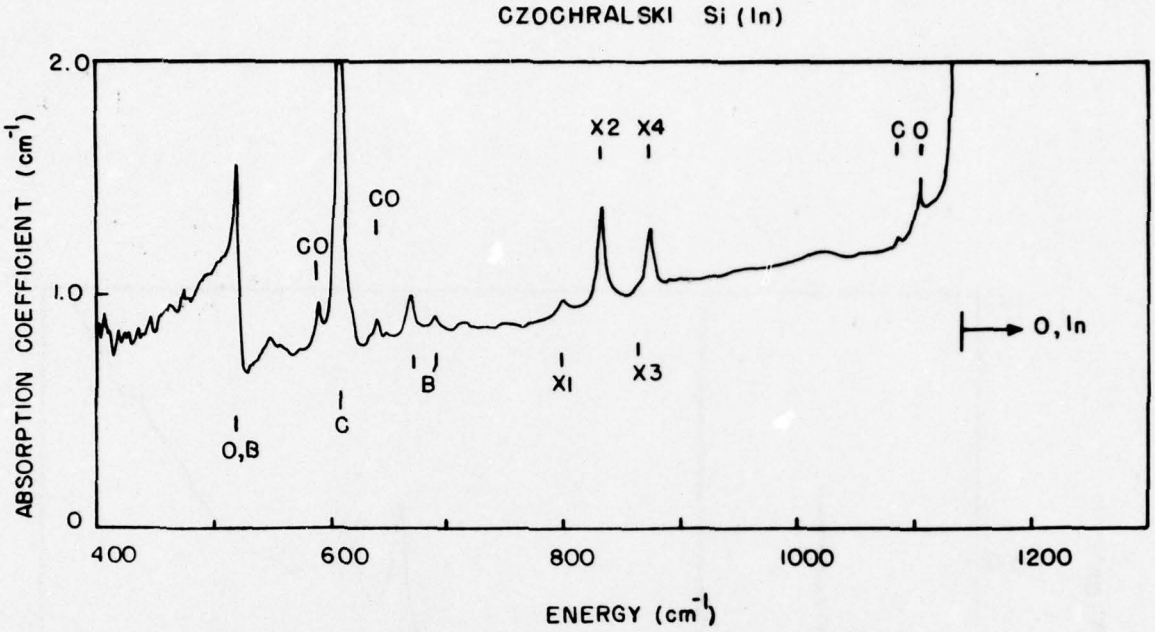

Figure 14. Absorption Spectrum in the Region of the X Defect in a Czochralski-Grown Indium-doped Silicon Crystal with 2.8×10^{17} In/cm³

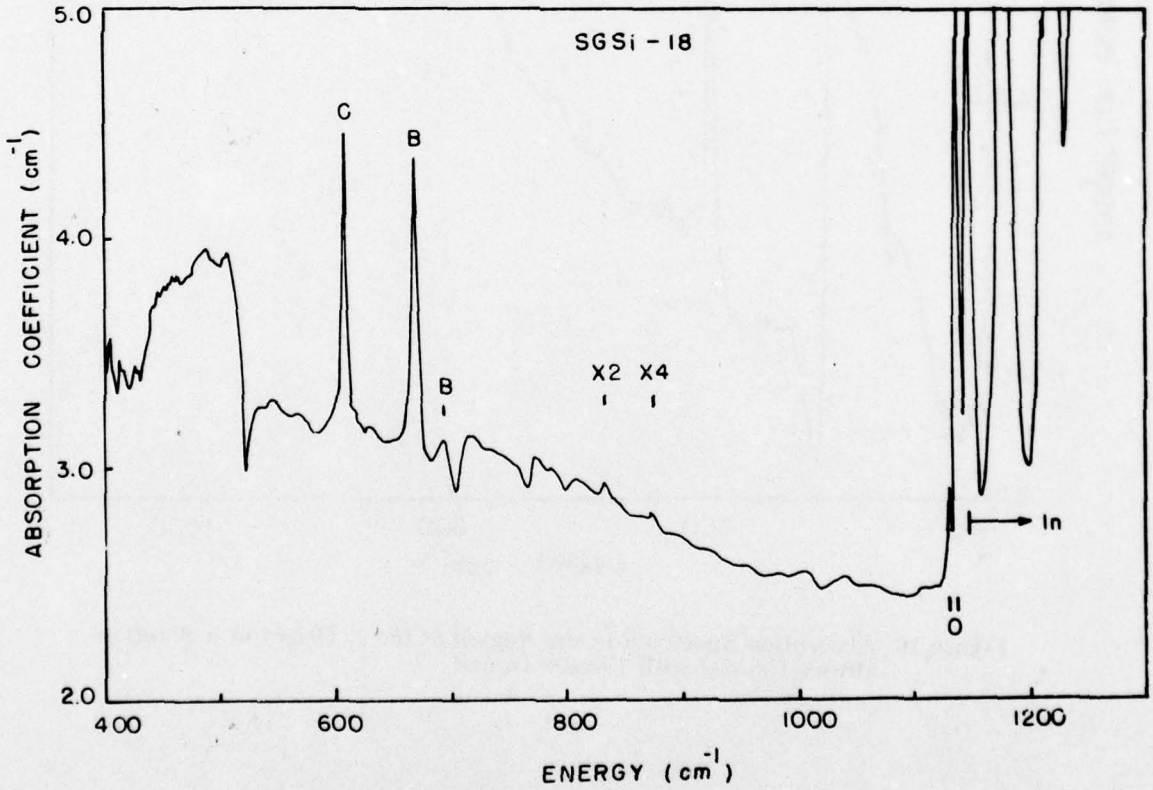

Figure 15. Absorption Spectrum in the Region of the X Defect in a Solution-Grown Crystal with 2.8×10^{17} In/cm³

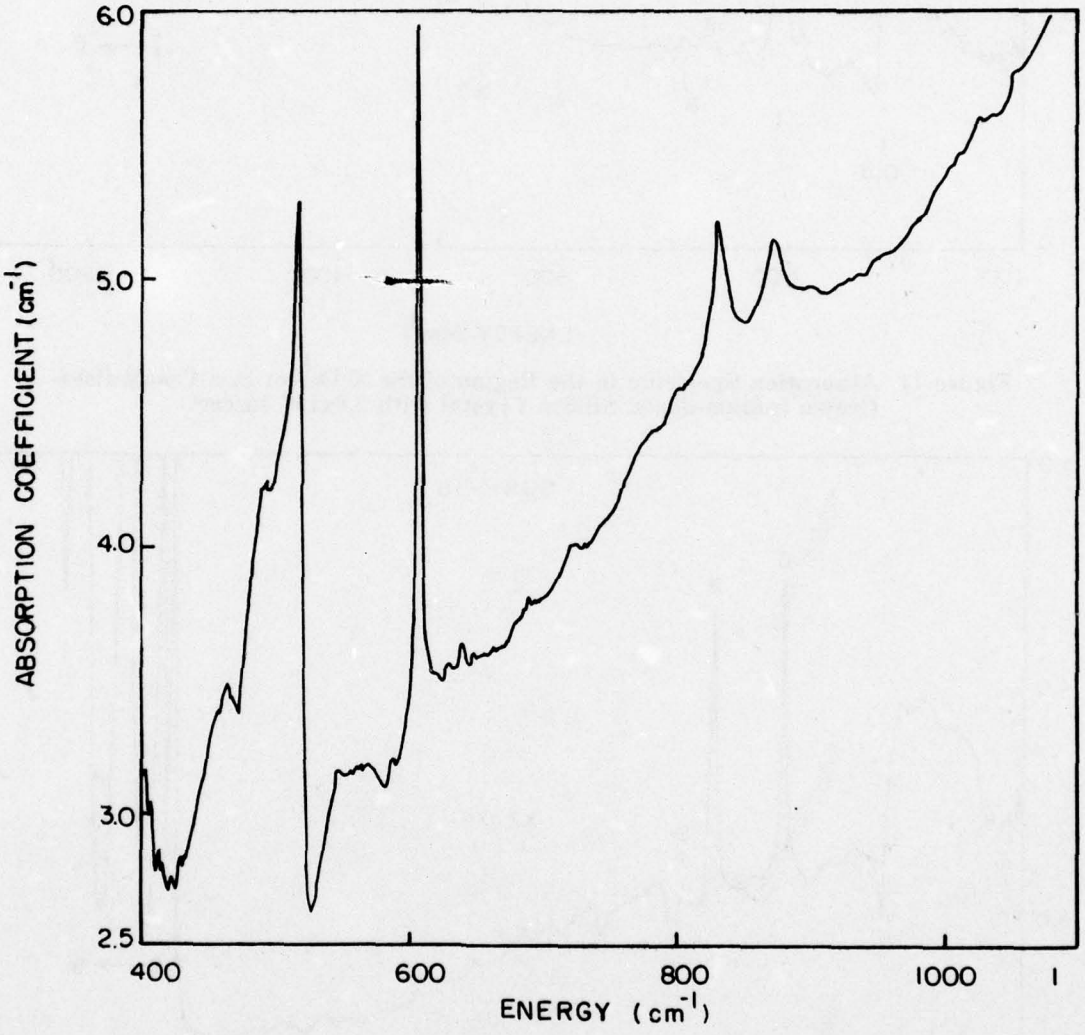

Figure 16. Absorption Spectrum in the Region of the X Defect in a Solution-Grown Crystal with 1.6×10^{18} In/cm³

The peak absorption coefficient for the various solution-grown crystals is shown in Figure 17 as a function of the growth temperature. Except for a normalizing factor (i.e., the optical cross-section), this is the same solubility curve shown in Figure 9. In this case, however, there has been no interpretation required in obtaining these values. The highest absorption coefficient we have obtained is 82 cm^{-1} in crystal SGSi-22. This is a most significant result and it indicates that very high quantum efficiency detectors can be made by using the solution-growth technique. As an example, if we make the photodetectors from a standard 0.017-inch wafer we can get 97 percent absorption of the nonreflected radiation in a single pass through the wafer.

The absorption cross section for the indium centers is listed in Table II for the various crystals grown in this program. The average value turns out to be 5.30×10^{-17} cm^2. The previous measurement of the cross section, 3.3×10^{-17} cm^2, was reported by Messenger and Blakemore.(7) In their interpretation they used a degeneracy of 6 for the indium ground state, which would tend to overestimate the indium concentration in their crystals. Using a degeneracy of 4 brings their cross section up in line with the value we observe.

Table II. Absorption Cross Section of Indium

Crystal	α peak (cm^{-1})	σ_{opt}
SGSi-12	7.6	5.07×10^{-17}
-15	3.01	5.54
-17	7.2	7.2
-18	15	5.35
-19	26	5.09
-20	42.5	4.25
-22	82	5.13
-23	67	4.78

Average $\sigma_{opt} = 5.30\times10^{-17}$ cm^2

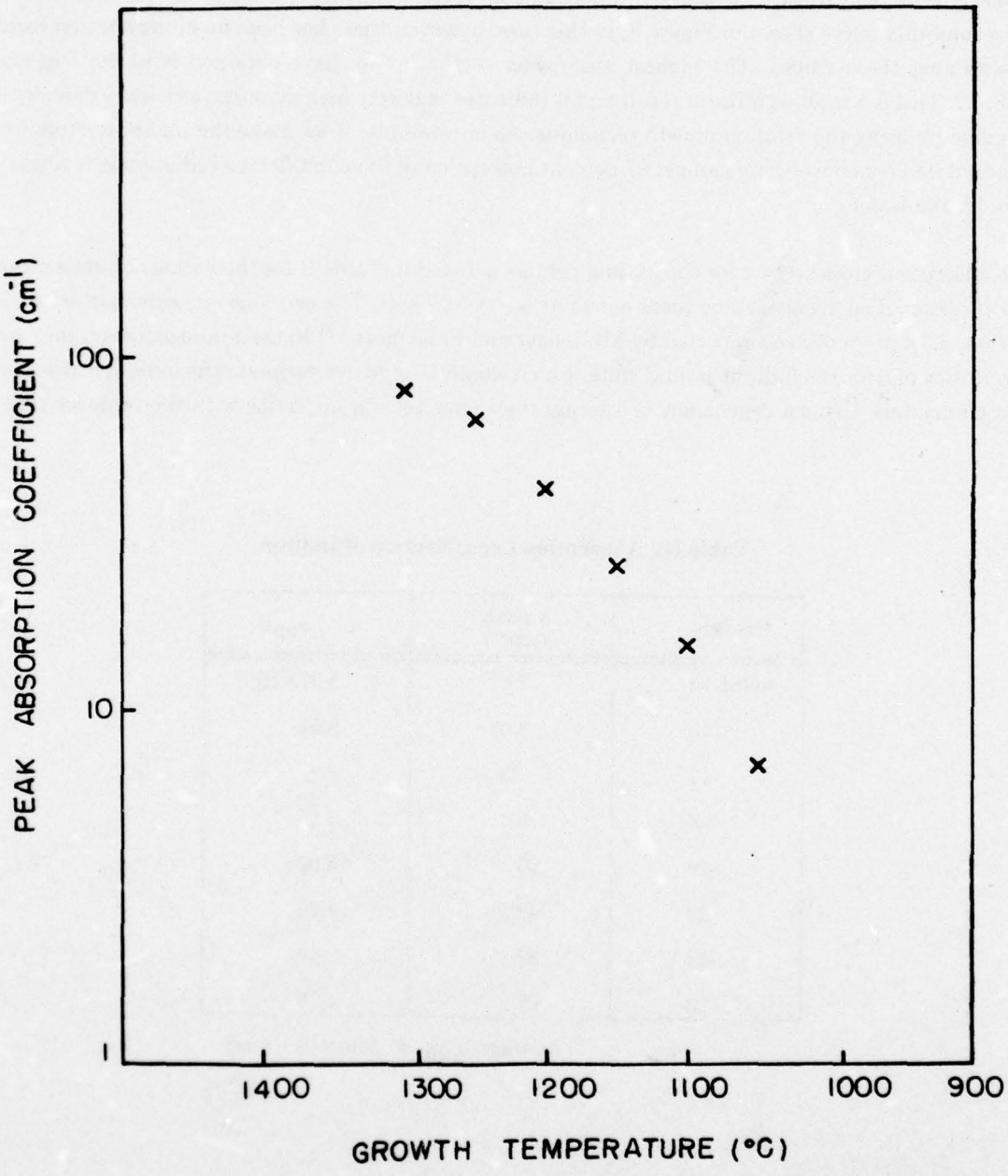

Figure 17. Peak Absorption Coefficient in Solution-Grown Indium-doped Silicon versus Growth Temperature

3.3.2 Spectroscopy of the Indium:X and Aluminum:X Defects

A summary of the infrared absorption measurements used to verify the existence of shallower acceptor levels in both indium-doped and aluminum-doped silicon is included in Appendix B. This is a copy of a paper written during this portion of the contract and accepted for publication in Applied Physics Letters.

3.3.3 Indium:X Concentration

The concentration of the indium:X defects in the various crystals measured is shown in Figure 18. The open circles are solution-grown crystals listed in Table I, and the triangles are Czochralski-grown crystals. The cross-hatched region in the figure is the range of results reported by Baron et al[8] on both Czochralski and float-zoned crystals.

The indium:X concentration in the solution-grown crystals is significantly lower than in comparably doped melt-grown crystals. Baron et al quoted a ratio of 0.005 for indium:X to indium, whereas the solution-grown crystals appear to be about a factor of 5 lower. There are not enough data to verify this precisely, but the general trend of a lower indium:X concentration is apparent in the solution-grown crystals.

The concentration of indium:X defects was obtained from the absorption measurements by assuming an integrated cross section of 3.5×10^{-15} cm for line 2 and is listed in Table III.

Table III. Summary of Optical Evaluations

Crystal	[In(X)] cm^{-3}	[B] cm^{-1}	α_{peak}, O_i cm^{-1}	α_{peak}, C cm^{-1}
SGSi-12		2.8×10^{15}	7.6	0.6
-15		1.6×10^{14}	1.5	0.01
-17		6.3×10^{14}	7.2	0.475
-18	2.2×10^{14}	6.3×10^{14}	15	1.28
-19	2.7×10^{14}	5.5×10^{15}	26	1.52
-20	5×10^{14}	1.5×10^{16}	42.5	1.8
-22	2.0×10^{15}	$<5\times10^{13}$	82	3.1
-23	2.0×10^{15}	4×10^{14}	67	3.3

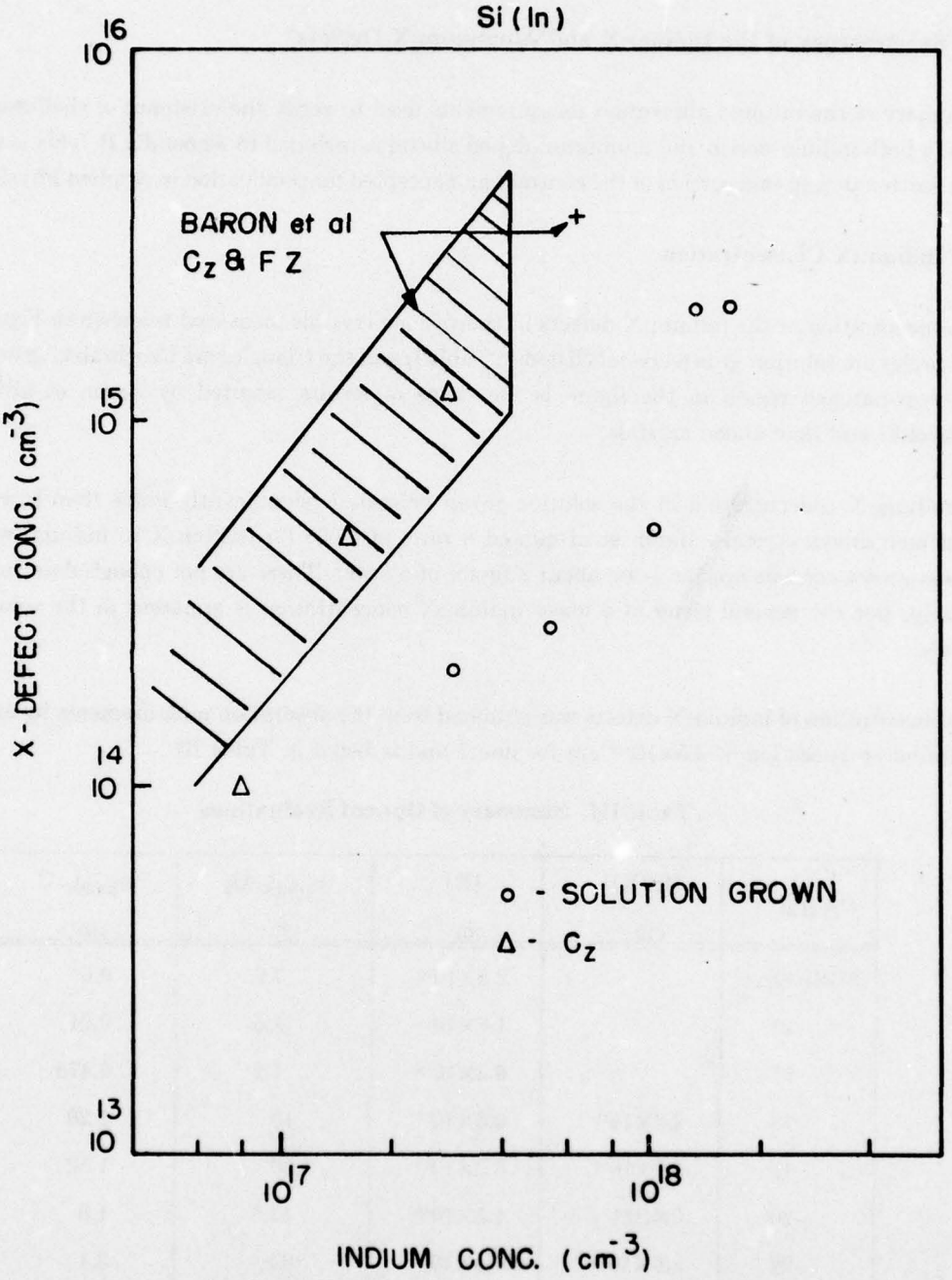

Figure 18. X Defect Concentration versus Indium Concentration

The fact that the results for Czochralski crystals agrees with the values reported by Baron et al was used as the validation of the accuracy of our technique. Regardless, the precision in determining the concentration is very good. Therefore, a direct comparison of the indium:X concentrations can be made between the Czochralski- and solution-grown crystals based on the optical measurements themselves. These also show a reduction factor of 5 in the indium:X concentration in solution-grown material.

3.3.4 Other Impurities

The other impurities which we could routinely measure with the optical measurements were boron, oxygen, and carbon as listed in Table III. In the case of boron, the concentration was determined from the integrated absorption intensity of the 668 cm^{-1} cm line and assuming an integrated cross-section of 6×10^{-15} cm. For the oxygen and carbon the results are left in terms of the peak absorption coefficient at 8K since we did not have a good calibration at low temperatures.

There is good correlation between the boron concentrations determined from the Hall data listed in Table I and from the optical measurements.

The oxygen and carbon concentrations appear to be increasing uniformly as the growth temperature is increased, indicating solubility limited values. The oxygen absorption intensity as a function of growth temperature is shown in Figure 19, and appears to be the solubility curve for oxygen in silicon. The absorption coefficient for a number of Czochralski crystals is also shown. It has been recognized that this value depends on the thermal history of the Czochralski crystals[9]) accounting for the range in values. The float-zoned crystal we measured was supplied by Dr. P. LoVecchio of the Night Vision and Electro-Optics Laboratory.

3.4 DEEP LEVEL TRANSIENT SPECTROSCOPY

Deep level transient spectroscopy (DLTS) is an important technique used in studying traps in semiconductors.[10,11] The DLTS technique has excellent sensitivity with defect concentrations as low as 10^{10}—10^{11} defects/cm^3 being observed.[12,13] Besides being used to measure trap concentrations, the technique can be used to determine trap parameters such as:

- Energy level
- Capture cross section
- Emission rate
- Optical cross section

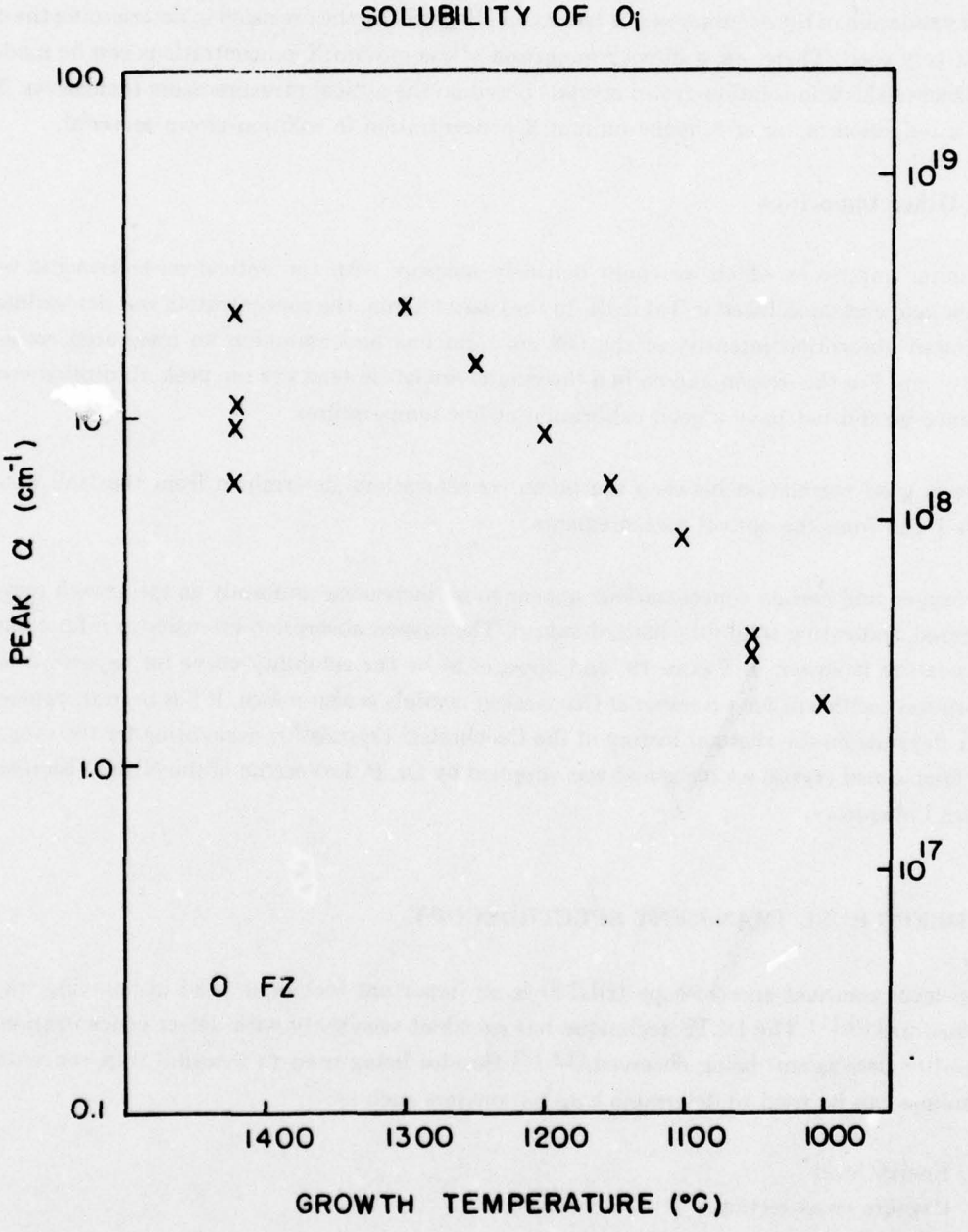

Figure 19. Solubility of O_i in Silicon

For indium-doped silicon these are the parameters needed to mathematically model the material as a photodetector. The energy levels and concentrations can be measured with optical absorption, photoconductivity, or Hall techniques, but the trapping cross sections and emission rates have not been well established.

Indium-doped silicon also has the shallower X defect level at 0.113 eV at concentrations approximately 0.005 times the indium concentration.[8] Even at these low concentrations this center affects the trapping and emission of free carriers and lowers the temperatures at which indium-doped silicon photodetectors can operate. This X defect is not easily detected in Hall or photoconductivity data. The infrared absorption data described in this report is the best characterization of this defect obtained to date.

The deep level transient spectroscopy (DLTS) effort for this contract has two main goals. The first is to identify the indium spectra in the DLTS data and to measure the trapping parameters for this dopant. The second goal is to see whether the DLTS technique can be used to monitor the X level and to characterize this defect's trapping parameters.

In the following sections a description of the DLTS technique is given, current data is presented and discussed, and the directions of future efforts are indicated.

3.4.1 Theory

During the measurements, the junction being investigated is maintained at some preset reverse bias except for short pulses of lower reverse bias or forward bias. The sequence of these voltage pulses and the measured capacitance transients are shown in Figure 20 along with a band diagram showing trapping in a p^+-n diode with donor traps. Indium in silicon would be similar except that acceptor trapping on the p side of the junction would be occurring. In reverse bias a region with no free carriers is set up, called the depletion region. The defects in this region are ionized in equilibrium, leaving a net positive charge on the n side and a negative charge on the p side producing a capacitance

$$C = \sqrt{\frac{e\epsilon}{2V}\,(N_{donors} - N_{acceptor})} \qquad (10)$$

where e is the electronic charge, ϵ is the permittivity, V is the applied plus the built-in diode voltage, and the N's are the dopant concentrations on the lightly doped side of the junction.[14]

With reference to Figure 20, when the shorter reverse bias pulse is applied, the depletion region contracts from its steady state value. Free carriers move into the previously depleted region and some of these are trapped. After the pulse, the carriers trapped on the very shallow centers are emitted immediately and those on the deeper traps are emitted more slowly. This produces an exponential change in the capaci-

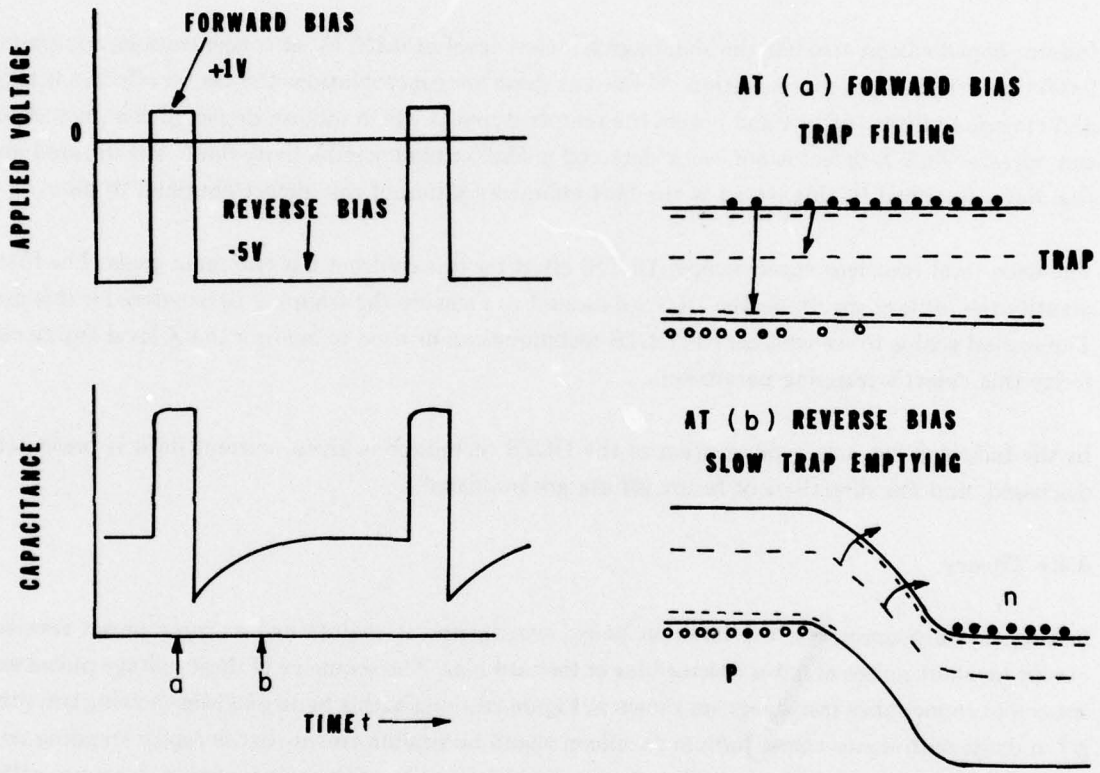

Figure 20. The applied voltage is shown in the top left and the resultant capacitance transient is shown below this. The right hand side of the figure shows the band structure for a p^+n diode with deep donor trap at the times (a) when the trap is filled during the pulse and (b) when the trap is emptying.

tance with a different decay time and amplitude for each trap. The DLTS apparatus decomposes the total capacitance transient into separate peaks for each trap. The magnitude of a peak is related to that trap's concentration by

$$N_T = 2(N_D - N_A) \frac{\Delta C}{C_o} \frac{\Delta w}{w_o} \tag{11}$$

where N_T is the trap concentration, $(N_D - N_A)$ is the net impurity charge per unit volume on one side of the junction, ΔC is the capacitance change due to one component of the transient, C_o is the steady state capacitance, Δw is the depletion width change during the pulse, and w_o is the steady state depletion width.

The emission of the trapped charge is a thermally activated process. The DLTS systems measures τ emission for each trap as a function of temperature. The trap energy can be found for hole traps by fitting the formula

$$T^2\tau = \frac{e^{\Delta E_T/KT}}{\sigma\left(\frac{2K^2 m^*}{\pi^2 h^3 g}\right)} \tag{12}$$

where T is the temperature, τ is the emission time constant, ΔE_T is the trap energy, and σ is the capture cross section.

In many pulsed capacitance techniques the capture cross section is also obtained from this formula. Partly because of electric field effects in the depletion region and partly because σ can vary with temperature, the capture cross sections calculated from Equation (12) have often been one to two orders of magnitude high.[9,10]

A more accurate way of measuring σ is to vary the filling pulse width. If the pulse is very short the free carriers are moved into the depletion region and out again before many traps can fill. As the pulse is held on for longer and longer times, more and more of the traps fill until saturation is reached. This shows up in the amplitude of the peak height seen in the DLTS data. The time constant for saturation (τ filling) is related to the capture cross section by

$$\tau_f^{-1} = \sigma \langle v \rangle n \tag{13}$$

where τ_f is the trap filling time constant, σ is the capture cross section, <v> is the average free carrier velocity (<v> = $8\,KT/\pi m^*$), and n is the free carrier concentration. The value of τ_f is taken from the filling time at which the peak amplitude equals ~0.63 saturation value. The value of <v> is calculated and n is measured as a function of temperature by Hall techniques. The capture cross section determined from Equation (13) depends on a minimum of parameters and is measured from trapping in the neutral crystal. The accuracy of this technique is much better than evaluating σ using Equation (12).

3.4.2 DLTS Spectrum

A DLTS spectrum for indium-doped silicon is shown in Figure 21. The DLTS spectrometer was set to respond to a certain emission rate. The emission rate for each trap varies with temperature. A shallow trap shows up as a peak at low temperatures while a deeper trap needs to be heated to a higher temperature to emit at the set DLTS rate. The amplitude of the peak is related to the trap concentration. The temperature at which a peak occurs is related to the trap energy and capture cross section through Equation (12). The direction of the peak (up or down) depends on whether the trap is a hole trap or an electron trap. All of the peaks shown in Figure 21 are due to hole traps.

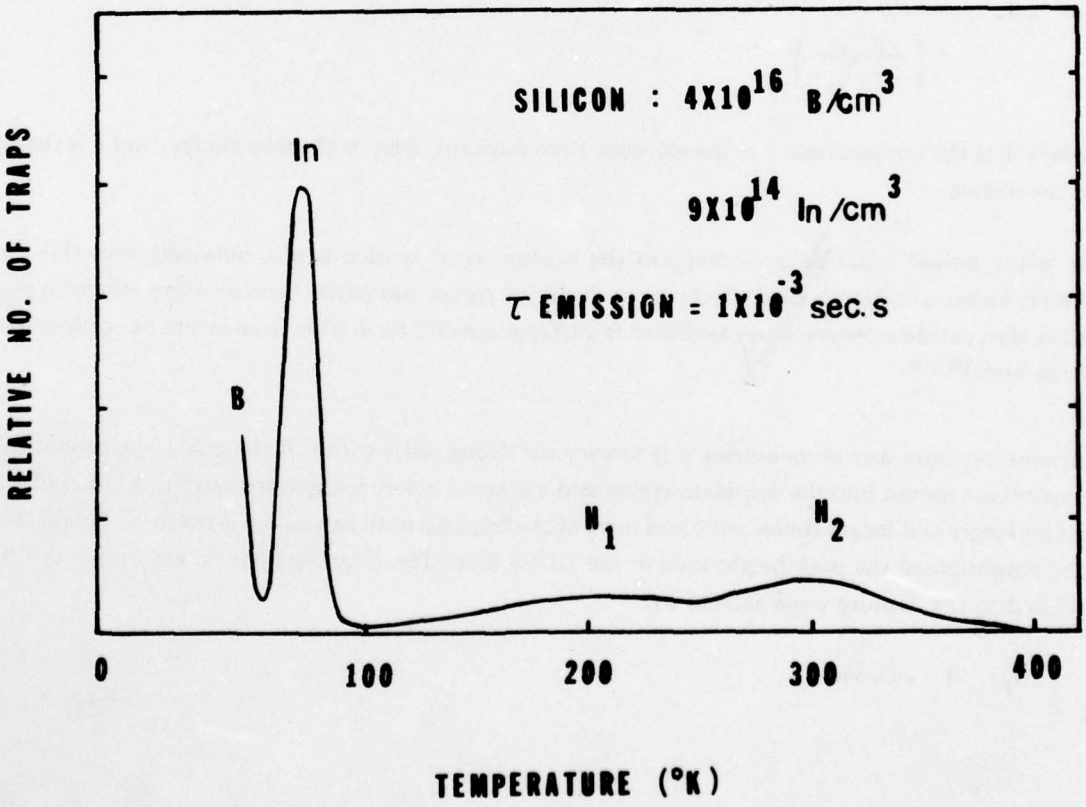

Figure 21. The DLTS Spectra Obtained for Indium-doped Silicon

The concentrations of the traps shown are:

$In \sim 3\times10^{15}$ traps/cm^3
$H_2 \sim 3\times10^{14}$ traps/cm^3
$H_1 \sim 1\times10^{14}$ traps/cm^3

The emission rate for holes trapped on indium in silicon is given in Figure 22 as a function of temperature. Figure 23 plots this data to fit Equation (12). The slope of each line gives the net thermal activation energy for each trap. If the capture cross section is a function of temperature, which it often is, it should be expressed in the form $\sigma = \sigma_0 \exp(\Delta E\sigma/KT)$. The net thermal activation energy given by the slope of the data in Figure 23 is then

$$\Delta E_{slope} = \Delta E_T - \Delta E_\sigma \tag{14}$$

The net thermal activation energy for each peak is

Peak	ΔE_{slope} (eV)
B	0.052
I_n	0.12
H_1	0.32
H_2	0.45

It was mentioned in the last section that capture cross sections are often calculated using Equation (12) but that the values obtained are often one to two orders of magnitude high. This is because the data is taken from emission in the depletion region, which is a nonequilibrium process in a region in which there are large fields. With this warning, the σ calculated from Equation (12) is

$$\sigma = 10^{-13}\ \text{cm}^2\ e^{0.04\text{eV}/KT} \tag{15}$$

or $\sigma \simeq 10^{-11}$ cm^2 at 80K. Again these numbers are expected to be high.

Because of the inaccuracy possible in the previous method it is of great interest to measure σ using the variable filling pulse method available in the DLTS technique. The data from this measurement is taken from the neutral material obtained when the depletion width is decreased and involves a more direct measurement of the capture cross section.

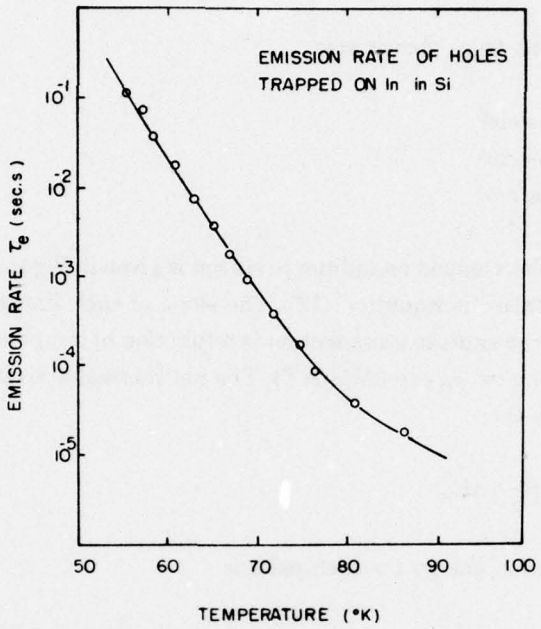

Figure 22. Emission Rate for Holes Trapped on Indium as a Function of Temperature

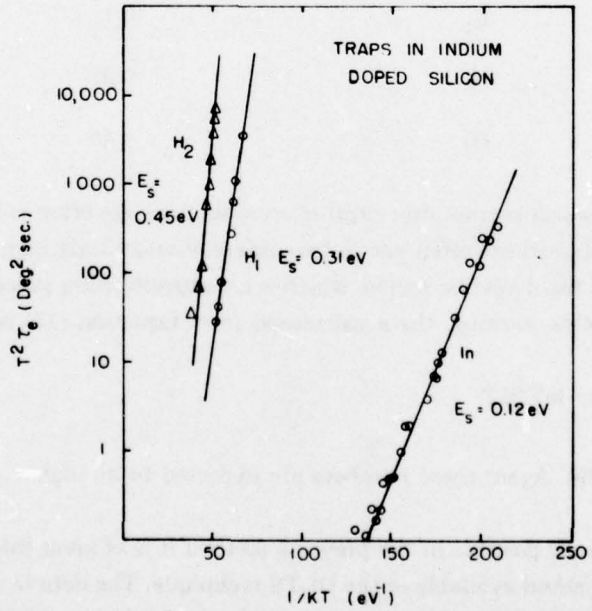

Figure 23. Determination of Trap Activation Energies from a Plot of $nT^2\tau$ versus 1/KT

The data for three different temperatures are shown in Figure 24. There is some scatter to this data, but the time constant for filling the traps is approximately constant for the temperatures shown and equal to $\sim 1.5 \times 10^{-8}$ sec. The capture cross sections calculated from Equation (13) are:

$$\sigma = 1.7 \times 10^{-15} \text{ cm}^2 \text{ at } 85\text{K}$$
$$2.9 \times 10^{-15} \text{ cm}^2 \text{ at } 75\text{K}$$
$$6.1 \times 10^{-15} \text{ cm}^2 \text{ at } 68\text{K}$$

This data is lower than that calculated from Equation (12), as was expected. More important, this data shows a slight temperature dependence which can be fit to the form

$$\sigma = \sigma_0 \exp(\Delta E_\sigma / KT) \text{ where } \Delta E_\sigma \simeq 0.04 \text{ eV}$$

3.4.3 Identification of the Indium Peak

The peak labelled In in Figure 23 is the only major peak which has appeared in all of the indium-doped samples prepared. Its effective activation energy has always shown up to be 0.115 to 0.120 eV, which was unexpectedly low compared with the value of 0.155 eV obtained by optical absorption, photoconductivity, and Hall measurements for In. The concentration estimated from the DLTS data of $\sim 3 \times 10^{15}$ traps/cm^3 compares well with the estimated indium concentration of 1×10^{15} In/cm^3 obtained from optical absorption and from the doping level added to the growth melt.

The concentration of this trap is also much too large to be the InX level, even though the effective thermal activation energy is closer to 0.1128 eV measured for this defect.

It is the temperature dependence of the capture cross section that resolves the energy picture. From Equation (14), given the measured total activation energy of $\Delta E_S = 0.12$ eV, and the capture cross section activation energy of 0.04 eV, the trap energy is found to be 0.16 eV, which fits the indium level.

3.4.4 The H_1 and H_2 Peaks

The peak near room temperature in Figure 23 labelled H_2 has an effective activation energy of ~ 0.45 eV and a concentration of $\sim 3 \times 10^{14}$ traps/cm^3 in the sample measured. This is the energy of the boron-vacancy complex. The crystal has a boron concentration of 5×10^{16} B/cm^3 and is unannealed so that strains near the pn junction act to produce vacancies.

The peak labeled H_1 is a hole trap at 0.32 eV above the valence band with a concentration of about 1×10^{14} traps/cm^3. In order to firmly determine models for these centers a much more extensive program involving

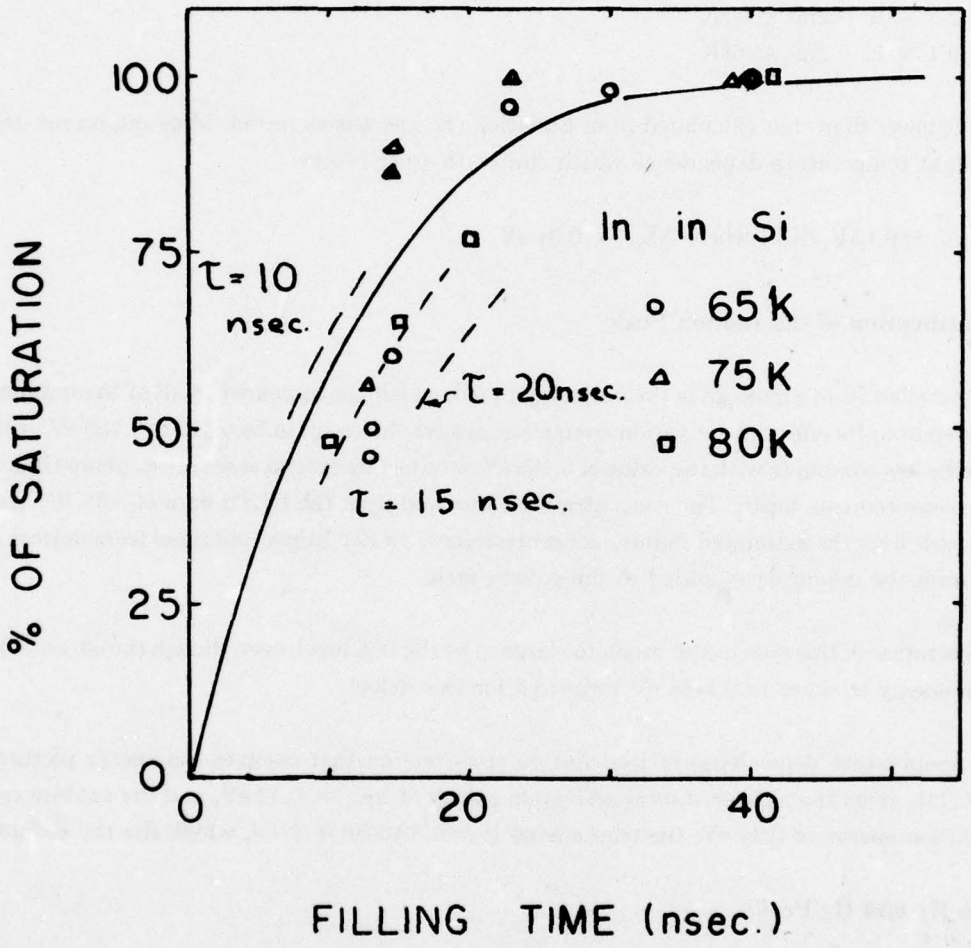

Figure 24. The amplidue of the In DLTS peak as a function of trap filling time. Curves for τ_f equal to 0.5 nsec, 1 nsec, and 2 nsec are shown for comparison.

the doping dependence, annealing rate, and comparisons with optical and spin resonance data would have to be made.

3.4.5 X Level

A second low temperature peak with an activation energy of 0.11 eV was seen in one sample prepared with very high indium and boron concentrations ($\sim 10^{16}$ In/cm^3 and $>10^{17}$ B/cm^3). This has not shown up in any other sample, so we are not at all sure we have seen the X level. This level should give a DLTS peak near the indium peak, but its exact position depends on the capture cross section. The peak observed was at slightly lower temperature than the indium peak, implying a very large capture cross section. The concentration of the X levels at ~0.005 times the indium concentration[7] means that the In peak may swamp the X peak in the spectral data. A double pulse technique which will largely cancel out the indium peak is being considered.

3.5 ORIGIN OF THE INDIUM:X DEFECT

A major concern throughout this contract is the identification of the indium:X defect. At the present time we have not been able to determine the origin of this shallow center. The work of Baron et al[8] suggests that this defect is not related to oxygen since it was observed in vacuum float-zoned crystals. In our crystals the indium concentration, the indium:X concentration and the oxygen concentration are all increasing with growth temperature, so oxygen cannot be ruled out on the basis of our work. In addition, the concentration carbon is increasing with growth temperature, so it also cannot be ruled out in our experiments.

Models for the indium:X defect include the following: indium as a single interstitial, indium in substitutional-interstitial pairs, indium next to another substitutional atom, and indium-vacancy complexes. These are grouped in Table IV along with the symmetries and the stress axis, giving the largest shift to the defect energy. In some of these defects, one particular type may have a number of different configurations. As an example, consider the interstitial impurity. It is known that boron interstitials bond into the silicon structure between two substitutional silicons in approximately [111] bond centered site. Oxygen commonly occupies a bond centered interstitial site and carbon can have this configuration, but usually only after irradiation. A split [100] substitutional configuration where two atoms sit off one substitutional site in the [100] direction is close to this in energy and should also be considered. Aluminum interstitials in a tetradedral void site have been observed. These are known to act as double donors (i.e., Al^o, Al^+, and Al^{++} are expected depending on the Fermi energy). Carbon, boron, and indium all sit preferentially on substitutional sites, but given the low concentration of X defects, the other sites may have to be considered. The single vacancy is not stable at room temperature but complexes with another vacancy, possibly carbon, boron, or aluminum, have been seen, mostly after irradiation. These vacancy complexes usually anneal between 100° to 300°C, so are not observed in silicon crystals without irradiation.

Table IV. Summary of Some Possible X Defects

Defect Class	Description	Symmetry	Stress-Energy Axis
I. In_i	Interstitial In		
	Tetrahedral	T_d	Symmetric
	Bond centered	D_{3d}	Off 111
	Split 100	D_{2d}	100
II. In_s-A_s	Substitutional Neighbors A = In, C, or B	C_{3v}	111
III. In_s-A_i or In_i-A_s	Substitutional-interstitial pair. Interstitial in tetrahedral site (A = Al or In)	C_{3v}	111 Off 111
	Bond centered or split 100 site (A = C, B, or O)	C_{2v}	100
IV. In_s + Vac.	Indium substitutional next to one or two vacancies	C_{3v}	
In_s + Di - vacancy		?	Off 111 or 110 (both possible)

During the next phase of the contract we will determine if the X defect can be observed in silicon doped with gallium or boron. This will give us some indication if the X defect is a problem with all the Group IIIA acceptors. In addition, piezospectroscopic measurements will be made on aluminum-doped silicon to determine the point symmetry at the acceptor. This should also help in narrowing down the number of possible complexes which could be responsible for the X defects. Experiments will also be done to vary the vacancy concentration in the crystals to determine if this has any influence on the concentration of X defects.

SECTION 4
ACCOMPLISHMENTS AND CONCLUSIONS

During this phase of the contract, significant information has been obtained concerning the growth and properties of indium-doped silicon. The major conclusion we have reached is that the gradient-transport solution growth is a feasible approach for growing more heavily doped crystals with a lower indium:X concentration than obtained in melt-grown crystals. The following is a list of the specific accomplishments of our research.

- Demonstrated the feasibility of growing Si(In) by the gradient-transport solution growth technique
- Determined the solubility limits of In in Si over the 950 to 1300°C temperature range
- Determined the maximum solubility of indium to be $1.6 \times 10^{18}/cm^3$
- Determined the maximum optical absorption coefficient in Si(In) to be 82 cm^{-1}. (Note: This value is not subject to an interpretive model, as is the doping level.)
- Observed five effective-mass-like excited states associated with the shallower indium:X defect at 112.8 meV
- Observed four effective-mass-like excited states associated with the shallower aluminum:X defect at 56.3 meV
- Determined the solubility limits of O_i in Si over the 1000 to 1300°C temperature range
- Observed the indium levels in DLTS spectra.

APPENDIX A
Si-In LIQUIDUS

An accurate knowledge of the Si-In liquidus is required in order to calculate the growth rate of silicon from solution. Thurmond and Kowalchik[16] have shown that the liquidus of many Si-metal systems, such as Si-In, are given by the expression

$$T = \frac{\Delta H_1^f + a\,(1-x_1)^2}{\Delta S_1^f - R\ln x_1 + b(1-x_1)^2}$$

where

T is the absolute temperature

x_1 is the atom fraction of Si in solution

ΔH_1^f is the latent heat of fusion of Si = 12.1 kcal/mole

$\Delta S_1^f = \frac{\Delta H_1^f}{T_1^f}$ = 7.19 kcal/mole°K

T_1^f is the fusion temperature of Si = 1683K

R is the gas constant

a is a fitting parameter = 11.45 kcal/mole

b is a fitting parameter = 3.37 cal/mole

The calculated liquidus is shown in Figure A1 along with the measured values of Thurmond and Kowalchik. The error bars on their data correspond to the range in the Si atom fraction in solution which they measured at each temperature. The calculated curve fits their data very well, but no data is available closer to the Si melting point.

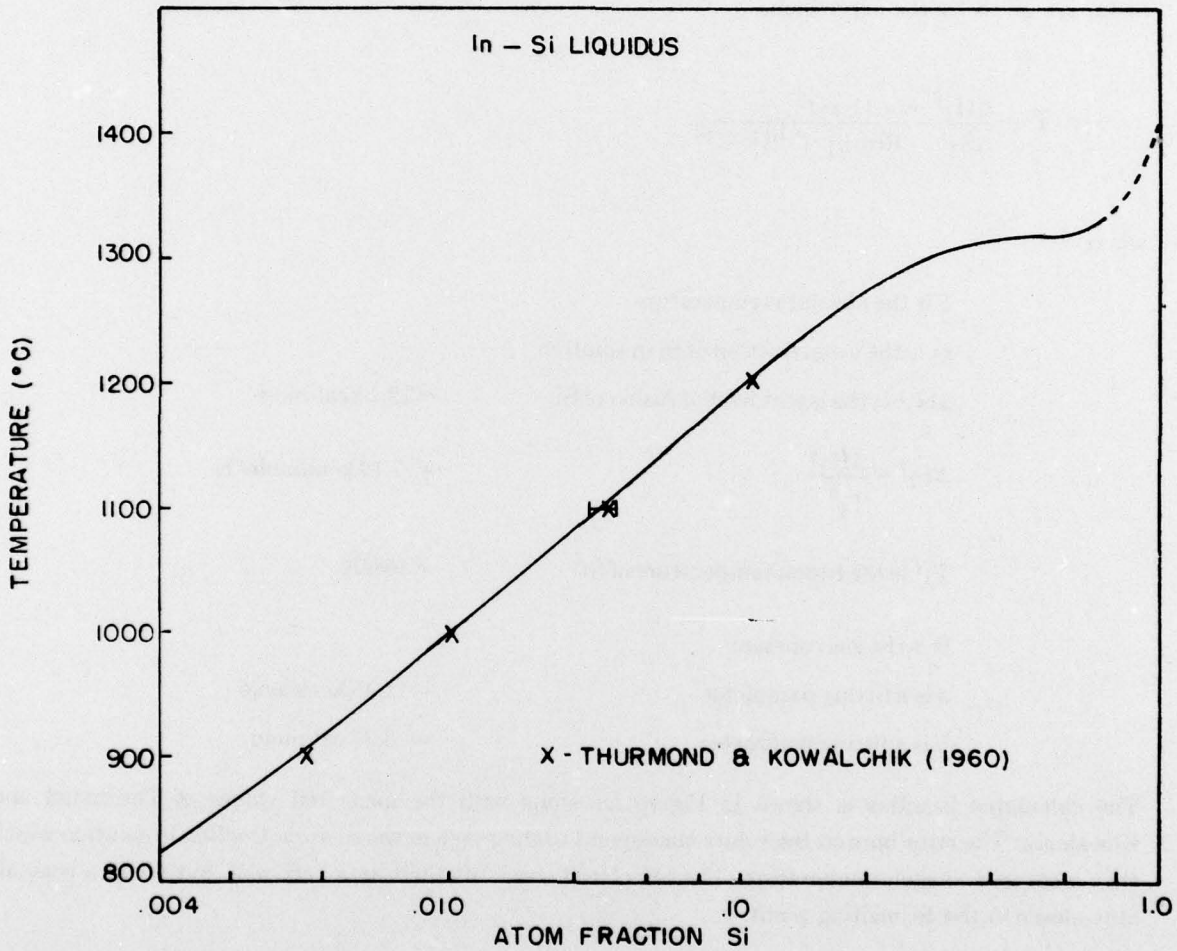

Figure A1. The Calculated Liquidus Curve and the Measured Values of Thurmond and Kowalchik

APPENDIX B

INFRARED SPECTRA OF NEW ACCEPTOR LEVELS IN INDIUM- OR ALUMINUM-DOPED SILICON*

Walter Scott

Honeywell Corporate Material Sciences Center
10701 Lyndale Ave. So., Bloomington, MN 55420

ABSTRACT

Infrared absorption measurements have verified the existence of shallower acceptor levels associated with both indium and aluminum in silicon. The new spectra correspond to effective-mass-like acceptors with optical ionization energies of 112.8 ± 0.3 meV indium-doped silicon and 56.3 ± 0.3 meV in aluminum-doped silicon. The existence of the shallower acceptor level in aluminum-doped silicon has been further verified by Hall coefficient measurements.

*Work supported in part by the Defense Advanced Research Projects Agency and the U.S. Army Night Vision and Electro-Optics Laboratory.

Electrical transport measurements in indium-doped silicon recently reported by Baron et al[17] indicate the presence of a shallower defect associated with the indium. The clearest indication of this defect came from low temperature Hall coefficient measurements. In some samples, freeze-out occurred with an activation energy of 111 ± 2 meV, but in other samples freeze-out occurred with an activation energy of 153 meV. The variation in the low temperature behavior was attributed to the presence of a shallower level at 111 meV in addition to the normal substitutional indium center at 153 meV. By changing the degree of compensation in the crystal, one can observe either the shallow level or the normal indium level at low temperatures. Baron et al were able to determine the concentration of this shallower defect by a detailed fit of the Hall effect data, and they concluded that this defect was present at a concentration of 0.5 percent of the indium concentration. They did not identify the nature of the defect involved, but suggested a complex of indium, such as pairs.

A similar discrepancy in the activation energy of aluminum-doped silicon exists in the literature, but has been ignored. The thermal activation energy of aluminum acceptors has for many years been quoted as 57 meV[18] but the optical ionization energy has consistently been measured as 68.5 meV.[5] Recently the thermal activation energy has been reported to be 67 ± 3 meV,[19] more in agreement with optical measurements. The various activation energies observed in aluminum-doped silicon can be accounted for by assuming more than one defect level influencing the electrical tansport measurements.

In this letter the results of optical absorption measurements are presented which clearly demonstrate the presence of additional shallower defects in both indium-doped and aluminum-doped silicon. These defects have an optical ionization energy of 112.8 ± 0.3 meV in indium-doped silicon and 56.3 ± 0.3 meV in aluminum-doped silicon. Hall coefficient measurements have also confirmed the existence of two levels in aluminum-doped silicon.

Samples were taken from Czochralski-grown crystals purchased from General Diode Corp[20] and also from crystals grown in our laboratories. The samples were lapped and polished with about a one-half degree taper to eliminate fringing and were cooled to 8K for transmittance measurements. The transmittance was measured using a Digilab FTS-14 Fourier transform spectrometer at a resolution of 2 cm^{-1} and converted to absorption coefficient in the usual way.[21] The samples were cooled to about 8K for measurement.

The absorption spectrum in the 780 to 920 cm^{-1} spectral range of an indium-doped crystal with $4x10^{17}$ In/cm^3 is shown in Figure B1. Five absorption lines are indicated by the dashes in the figure at energies of 799 cm^{-1}, 831 cm^{-1}, 863 cm^{-1}, 873 cm^{-1} and 891 cm^{-1}. The line at 863 cm^{-1} consist of a shoulder on the low energy side of the 873 cm^{-1} line, but is sufficiently separated to be distinguishable.

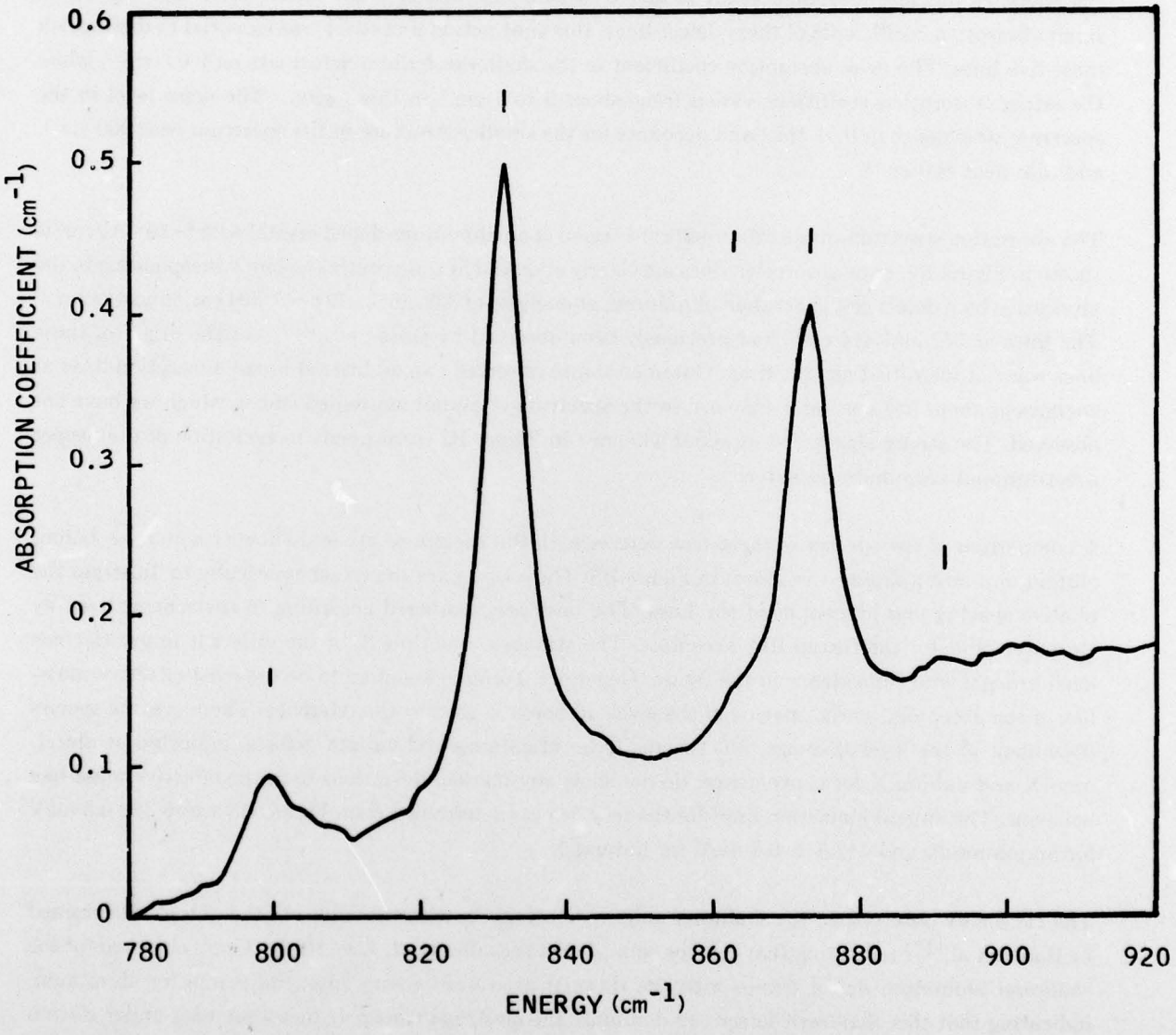

Figure B1. Absorption spectrum of the shallower indium acceptor at a temperature of 8K, in a crystal with 4×10^{17} In/cm^3. The silicon lattice lines in this region have been subtracted from the spectrum to show the lines.

The silicon lattice absorption lines normally observed in this spectral region[22] have been subtracted from the absorption spectrum in order to display the defect lines. The reference sample was a high purity vacuum float-zoned crystal without impurity absorption lines in this region. The absorption spectrum of the reference was also measured at 8K to give complete subtraction of the lattice lines. Because of the small absorption coefficients of these defect lines, this subtraction procedure was essential to distinguish these five lines. The peak absorption coefficient in the shallower indium defect was only 0.5 cm^{-1}, while the lattice absorption coefficient varied from about 5 to 7 cm^{-1} in this region. The noise level in the spectrum was less than 0.01 cm^{-1} and accounts for the smaller structure in the spectrum near 900 cm^{-1}, and also near 800 cm^{-1}.

The absorption spectrum in the 320 to 440 cm^{-1} region of an aluminum-doped crystal with $8x10^{16}$ Al/cm^3 is shown in Figure B2. Four absorption lines are clearly observed in this spectral region, corresponding to the absorption by a defect shallower than aluminum, at energies of 338 cm^{-1}, 372 cm^{-1}, 404 cm^{-1} and 414 cm^{-1}. The lines at 372 and 414 cm^{-1} had previously been observed by Onton et al[5], but the origin of these lines was not identified at that time. Onton et al also observed two additional broad absorption lines at energies of about 395 cm^{-1} and 488 cm^{-1} in the spectrum of aluminum-doped silicon which we have not observed. The strong absorption at about 440 cm^{-1} in Figure B2 corresponds to excitation of the deeper substitutional aluminum acceptor.

A comparison of the spectra of these new defects with the spectra of other shallow acceptors — boron, aluminum, and indium — is shown in Figure B3. The spectra are shown schematically to illustrate the relative spacing and intensities of the lines. The lines are numbered according to the scheme used by Onton et al[5] for the Group IIIA acceptors. The strongest line, line 2, of the different impurities has been brought into coincidence in the figure. Generally, boron is assumed to be the most effective-mass-like of the acceptors, so the spacing of the levels in boron is used as the reference. There is some species dependent in the level spacings, but the shallower aluminum and indium defects, indicated as aluminum:X and indium:X for convenience, do not show any marked deviations from the effective-mass-like behavior. The optical ionization limit for the new defects determined from Figure B3 are 56.3 ± 0.3 meV for aluminum:X and 112.8 ± 0.3 meV for indium:X.

The 112.8 meV observed for the shallower indium defect agrees with the value of 111 ± 2 meV determined by Baron et al,[17] indicating that it is the same defect they observed. Also, the 56.3 meV observed for the shallower aluminum defect agrees with the thermal activation energy often measured for aluminum, indicating that this shallower defect can dominate the electrical transport measurements under certain circumstances.

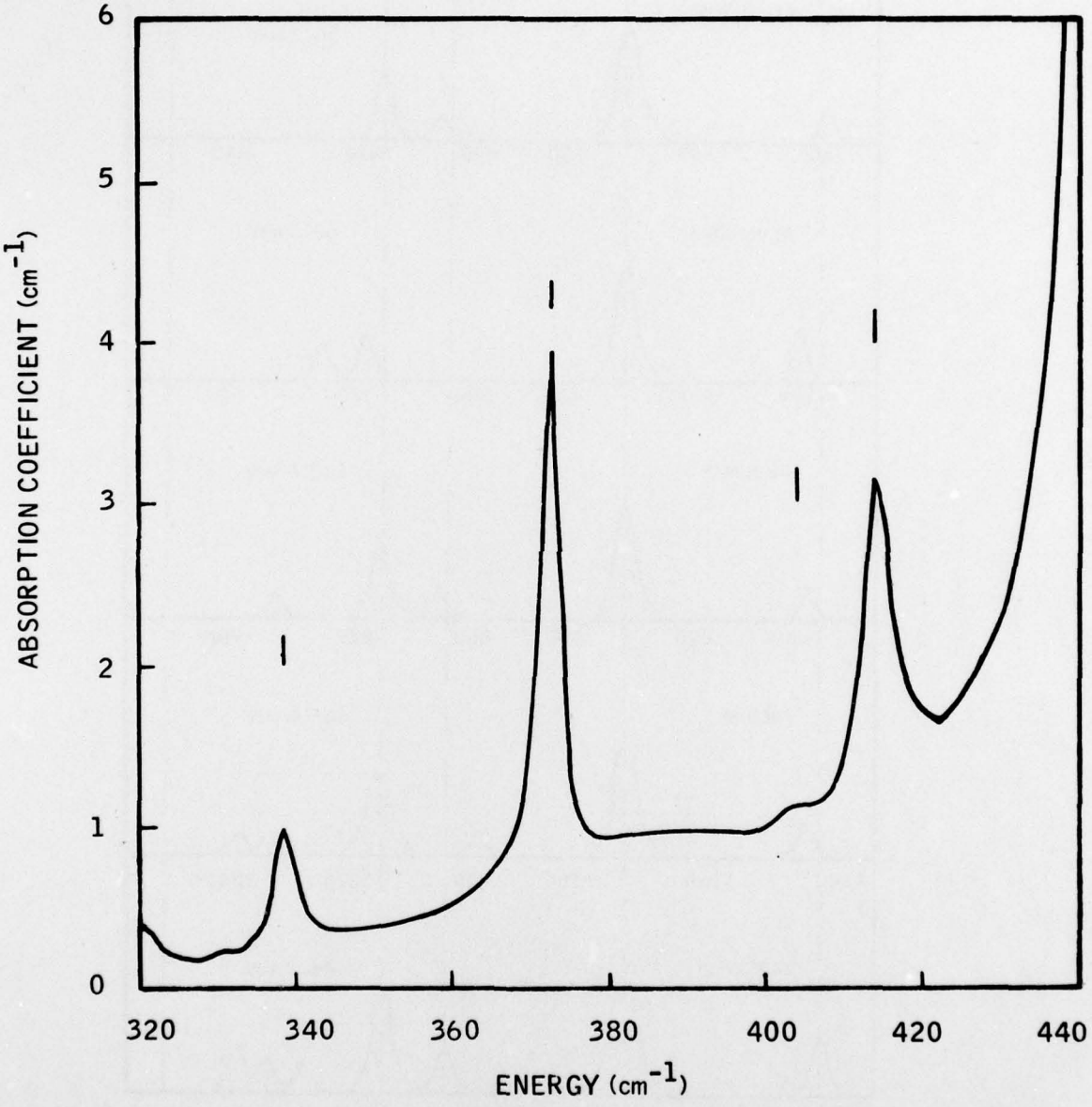

Figure B2. Absorption spectrum of the shallower aluminum acceptor at a temperature of 8K in a crystal with 8×10^{16} Al/cm^3

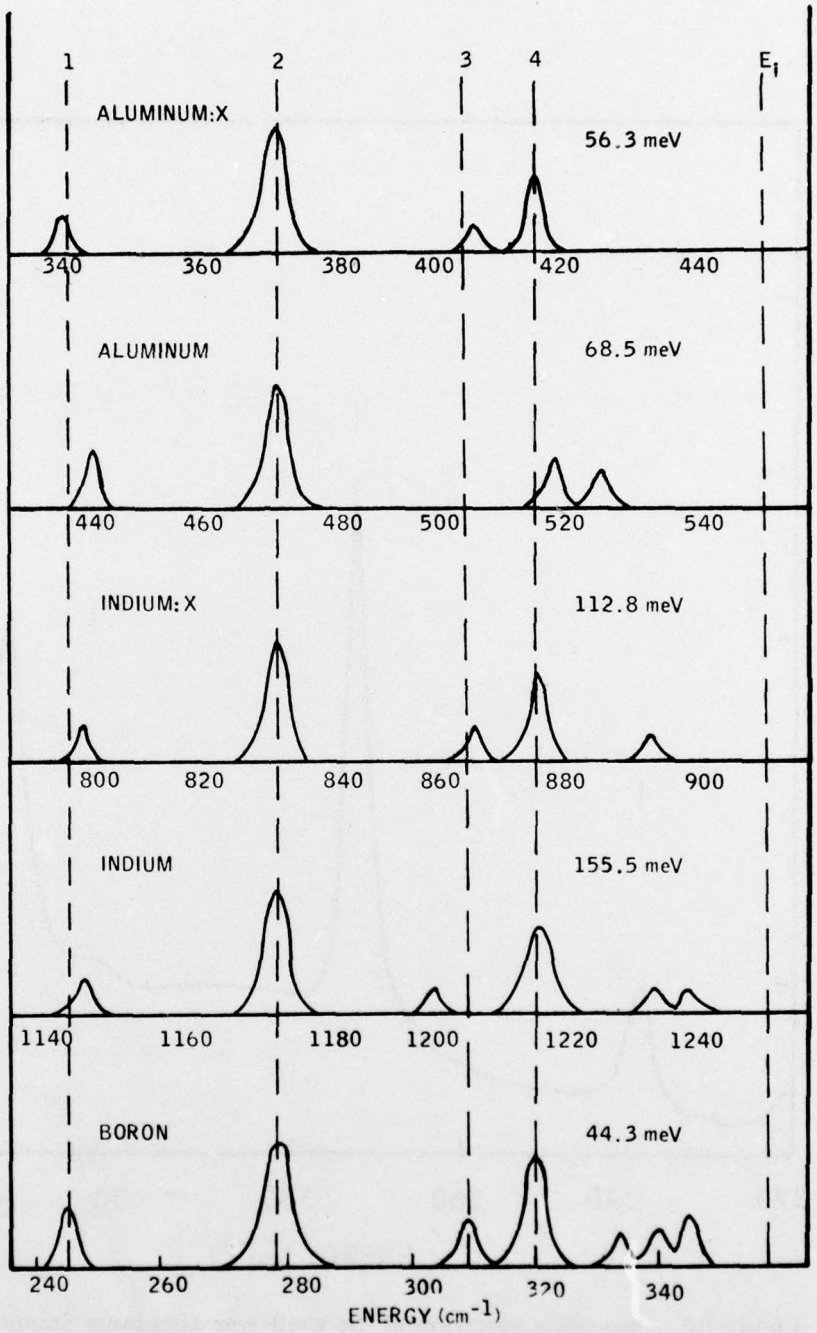

Figure B3. Relative spacing and relative magnitudes of the absorption lines of boron, aluminum, and indium compared with the new defects, designated as aluminum:X and indium:X

The existence of the new defect in aluminum-doped silicon was further verified by Hall effect measurements. Two different thermal activation energies corresponding to the 56.3 meV and 68 meV levels can be obtained in aluminum-doped crystals by adjusting the degree of compensation. To do the measurements on one Hall sample, the concentration of thermal donors was varied in order to vary the compensation level in the crystal.

Figure B4 shows the Hall coefficient as a function of reciprocal temperature for an aluminum-doped crystal after two different heat treatments. Initially, the crystal was heated at 410°C for 3 hours, resulting in a measured activation energy of 66 ± 1 meV. Subsequent heating at 750°C for 45 minutes reduced the measured activation energy to 56 ± 1 meV. The two activation energies obtained here correspond to the values for the aluminum thermal ionization energies previously reported by various authors,[5,18] and are simply explained in terms of two different acceptor levels.

It is well known[23] that a low temperature (about 400°C) heat treatment of Czochralski-grown silicon increases the number of donor centers in a crystal by generation of thermal donors. These donors compensate the acceptors, starting with the shallowest ones first. The three-hour anneal was sufficient to completely compensate the shallower aluminum:X defect, but not all of the deeper aluminum centers. The low temperature electrical properties are then determined by the deeper acceptor, giving an activation energy of 66 ± 1 meV. The activation energy is slightly lower than the optical ionization energy of 68.5 meV, but agrees with the value reported by Sclar.[19]

The high temperature (750°C) heat treatment removes the thermal donors so that the aluminum:X levels are no longer all compensated. The electrical transport properties at low temperatures are then dominated by this shallower defect at 56.3 meV, as found in Figure B4.

The Hall effect measurements were made using a standard high impedance dc Hall effect system[24] and a conventional bridge configuration for the sample. A detailed fit of the Hall effect data to accurately determine the compensation level was not done for these samples. In each case only the defect activation energy was obtained from the Hall measurements.

The concentration of the aluminum:X defect relative to the aluminum concentration was estimated from the relative absorption intensities of the aluminum and aluminum:X lines. The defect is present at a concentration of about 0.4 percent of the aluminum concentration, which is about the same as the ratio found in the indium-doped material.

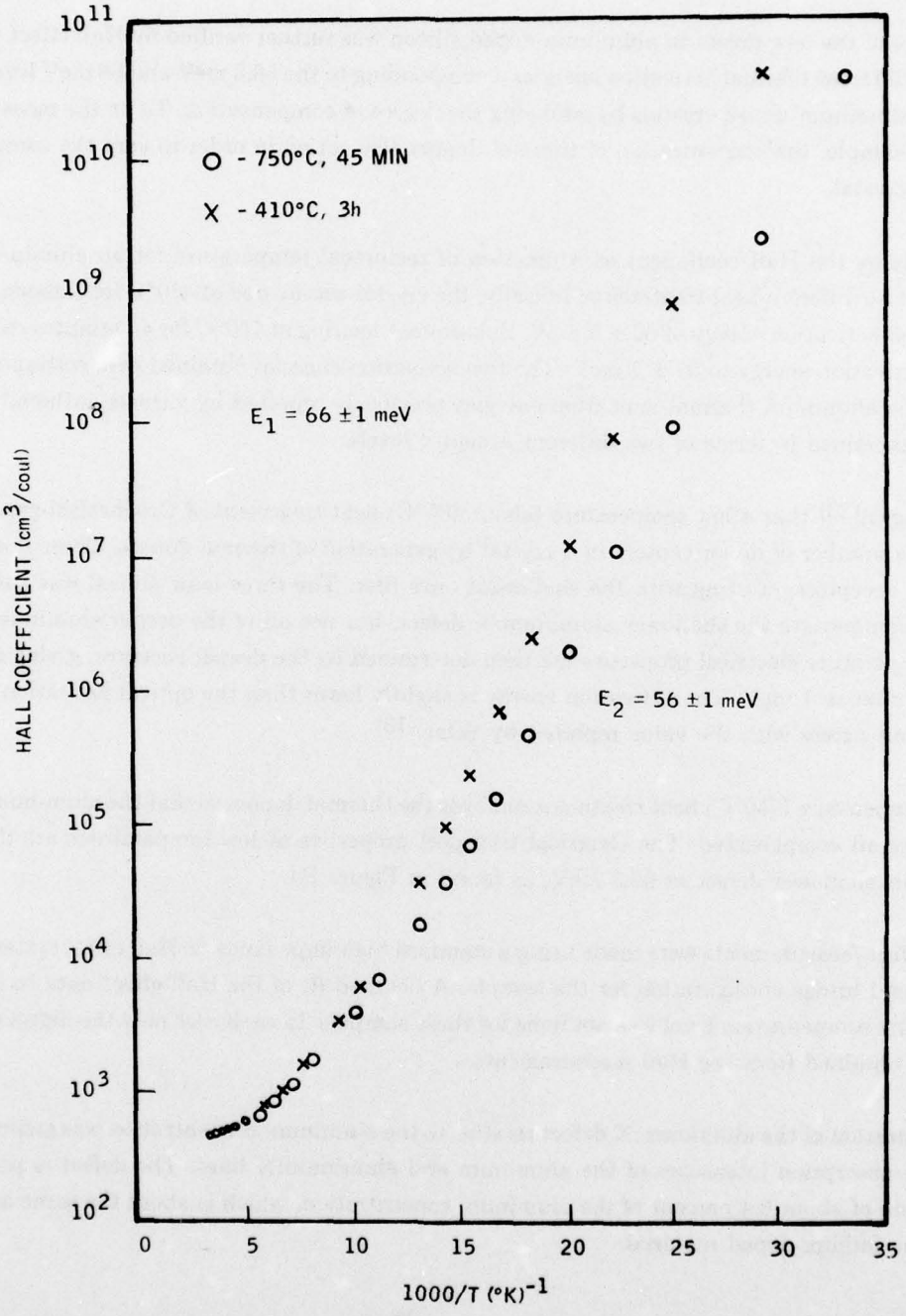

Figure B4. Hall coefficient as a function of reciprocal temperature for an aluminum crystal after two different heat treatments. The activation energies for the two cases are 66 ± 1 meV and 56 ± 1 meV.

No indication of the nature of these defects is available at this time. Onton et al[5] reported that these extra absorption lines were not present in float-zone grown material, so they suggested that they were due to an oxygen related defect. The aluminum concentration was also very low in the float-zone grown crystal used by Onton et al, so the extra lines would have been very difficult to detect. Baron et al[17] observed the indium-related defect in vacuum float-zoned crystals basically ruling out oxygen as the cause of the shallower defects. It is believed that these shallower defects observed in both indium- and aluminum-doped silicon have a common origin and that this type of defect associated with substitutional acceptors may be a common occurrence for all the Group IIIA impurities in silicon.

The author would like to thank J.E. Sjerven and R.J. Hager for assistance in the crystal growth and the electrical and optical measurements.

REFERENCES

1. The data for diffusion in liquids is summarized in the paper by N.H. Nachtrieb, Adv. Phys. 16, 309 (1967).
2. N. Sclar, IEEE Trans. El. Dev. ED-24, 709 (1977).
3. O.J. Marsh, Final Technical Report, Contract DAAK02-75-C-0079, sponsored by Night Vision Laboratory, April 1976.
4. H.D. Barber, S.S. El. 10, 1039 (1967).
5. A. Onton, P. Fisher and A.K. Randas, Phys. Rev. 163, 686 (1967).
6. G.D. Watkins and W.B. Fowler, Phys. Rev. B 16, 4524 (1977).
7. R.A. Messenger and J.S. Blakemore, S.S. Commun. 9, 319 (1971).
8. R. Baron, M.H. Young, J.K. Neeland and O.J. Marsh, Appl. Phys. Lett. 30, 594 (1977).
9. D. Helmreich and E. Sirtl, "Proceedings of the Third International Symposium on Silicon Materials Science and Technology," H.R. Huff and E. Sirtl, Eds. (The Electrochemical Society, Princeton, N.J., 1977), p. 626.
10. D.V. Lang, J. Appl. Phys. 45, 3014 (1974).
11. D.V. Lang, J. Appl. Phys. 45, 3023 (1974).
12. C.T. Sah, L. Forbes, C.L. Rosier, and A.F. Tasch, Jr., Solid-State Electronics 13, 759 (1970).
13. C.T. Sah, and A. Neugroschel, IEEE Trans. on Electron Devices 23, 2059 (1976).
14. S.M. Sze, Physics of Semiconductor Devices, Chapter 3, (Wiley-Interscience, New York) 1969.
15. G.C. Osbourn and D.L. Smith, Phys. Rev. 16, 5429 (1977).
16. C.D. Thurmond and M. Kowalchik, Bell Syst. Tech. J. 39, 169 (1960).
17. R. Baron, M.H. Young, J.K. Neeland and O.J. Marsh, Appl. Phys. Lett. 30, 594 (1977).
18. M.L. Schultz, Infrared Phys. 4, 93 (1964).
19. N. Sclar, Infrared Phys. 16, 435 (1976).
20. General Diode Corp., 9090 Eames Street, Framingham, MA 01701.
21. T.S. Moss, "Optical Properties of Semiconductors," Acadamic Press, New York (1959), p. 14.
22. R.J. Collins and H.Y. Fan, Phys. Rev. 93, 674 (1954).
23. W. Kaiser, H.L. Frisch and H. Reiss, Phys. Rev. 112,1546 (1958).
24. R. Baron, M.H. Young, J.K. Neeland and O.J. Marsh, "Proceedings of the Third International Symposium on Silicon Materals Science and Technology," H.R. Huff and E. Sirtl, Eds. (The Electrochemical Society Inc., Princeton, N.J., 1977) p. 367.